



HAL
open science

Reconstruction of anthropogenic activities in legacy sediments from the Eure River, a major tributary of the Seine Estuary (France)

Thomas Gardes, Maxime Debret, Yoann Copard, Edouard Patault, Thierry Winiarski, Anne-Lise Develle, Pierre Sabatier, André-Marie Dendievel, Brice Mourier, Stéphane Marcotte, et al.

► To cite this version:

Thomas Gardes, Maxime Debret, Yoann Copard, Edouard Patault, Thierry Winiarski, et al.. Reconstruction of anthropogenic activities in legacy sediments from the Eure River, a major tributary of the Seine Estuary (France). *CATENA*, 2020, 190, pp.104513. 10.1016/j.catena.2020.104513. hal-02504266

HAL Id: hal-02504266

<https://univ-lyon1.hal.science/hal-02504266v1>

Submitted on 7 Mar 2022

HAL is a multi-disciplinary open access archive for the deposit and dissemination of scientific research documents, whether they are published or not. The documents may come from teaching and research institutions in France or abroad, or from public or private research centers.

L'archive ouverte pluridisciplinaire **HAL**, est destinée au dépôt et à la diffusion de documents scientifiques de niveau recherche, publiés ou non, émanant des établissements d'enseignement et de recherche français ou étrangers, des laboratoires publics ou privés.



Distributed under a Creative Commons Attribution - NonCommercial 4.0 International License

1 **Reconstruction of anthropogenic activities in legacy sediments**
2 **from the Eure River, a major tributary of the Seine Estuary**
3 **(France)**

4

5 Thomas Gardes^{1,2,*}, Maxime Debret¹, Yoann Copard¹, Edouard Patault¹, Thierry Winiarski³,
6 Anne-Lise Develle⁴, Pierre Sabatier⁴, André-Marie Dendievel³, Brice Mourier³, Stéphane
7 Marcotte⁵, Barbara Leroy⁶, Florence Portet-Koltalo²

8

9

10 ¹Normandie Univ, Rouen, UNIROUEN, UNICAEN, CNRS, M2C, 76000 Rouen, France.

11 ²Normandie Univ, Rouen, UMR CNRS 6014 COBRA, 55 Rue Saint Germain, 27000 Evreux, France.

12 ³Université Lyon 1, ENTPE, UMR CNRS 5023 LEHNA, 3 Rue Maurice Audin, 69518 Vaux-en-Velin, France.

13 ⁴Université Grenoble Alpes, Université Savoie Mont Blanc, CNRS, EDYTEM, 73000 Chambéry, France.

14 ⁵Normandie Univ, Rouen, INSA de Rouen, UMR CNRS 6014 COBRA, Avenue de l'Université, 76801 Saint-
15 Etienne-du-Rouvray Cedex, France.

16 ⁶Agence de l'eau Seine-Normandie, Quai de Boisguilbert, 76000 Rouen, France.

17

18 *Corresponding author: thomas.gardes2@univ-rouen.fr

19

20 **Keywords:** Anthropogenic Activities, Eure River, Legacy Sediments, Sediment Cores, Trace
21 **Metals.**

22

23

24

25

26

27

28

29 **Abstract**

30

31 Most rivers worldwide are contaminated by various trace metals from different origins,
32 which may be stored for considerable periods of time in depositional areas. Most of these
33 studies are focused on the main river of a watershed and the tributaries are often neglected
34 which can be important sources of contamination. The aim of this study was to reconstruct the
35 anthropogenic activities that occurred in the Eure River, tributary of the Seine Estuary, since
36 the 1940s using "legacy sediments". The results showed that the temporal trends of trace
37 metals were not related to detrital inputs and TOC variations but with the industrial history of
38 the Eure River watershed. The high levels of Zn, Cu, and Ni during the 1950s and the 1960s
39 and the decrease with the decline of the probable main source of release showed the
40 watershed reactivity to anthropogenic activities. The high levels of Pb during the 1990s and
41 the 2000s showed that the watershed reacted immediately to anthropogenic pressures. The Pb
42 levels remained important after the cease of industrial activity, showing that a resilience
43 period is necessary for the system, and that interactions between human activities and the
44 environment go beyond of the activities themselves.

45

46 **1. Introduction**

47

48 Many researchers agree that the Earth has entered a new geological period, the
49 Anthropocene (Crutzen and Stoermer, 2000; Crutzen, 2006; Steffen et al., 2011; Lewis and
50 Maslin, 2015). While the beginning of this period is the subject of intense debate (Lewis and
51 Maslin, 2015), there is consensus that humans have seriously impacted their environment
52 during this period (Steffen et al., 2011). Such human activities as agriculture, forestry, mining,

53 and water storage and diversion contribute significantly to landscape change and
54 environmental contamination. The sediments generated by the erosive actions of humans have
55 received increasing attention in recent years and have even been categorised as a particular
56 type, known as legacy sediments (James, 2013, 2018); these are generally defined as alluvial
57 sediments that are deposited as a result of anthropogenic disturbances within a watershed
58 (James, 2013). Among the several sedimentation and storage zones throughout the watershed,
59 there is particular concern about how legacy sediments trapped behind dams are managed (i.e.
60 dredging). Structures such as dams change the flow of a river to achieve particular objectives
61 (e.g. energy production, flood control, and navigation) and serve to modify the hydrodynamic
62 cycle and thus the sediment storage in catchment (Nilsson et al., 2005; Yang et al., 2006).
63 Many studies have examined the storage of metallic and organic contaminants behind dams
64 (e.g. Shuman, 1995; Müller et al., 2000; Bednarek, 2001; Stanley and Doyle, 2003; Audry et
65 al., 2004; Ashley et al., 2006; Devault et al., 2009; Dhivert et al., 2015; Evans, 2015). Hence,
66 legacy sediments can be viewed as the industrial and agricultural testimonies of past
67 anthropogenic activities in, and can reflect the trajectory of, any studied watersheds. In
68 addition, estuaries are dynamic environments where it is difficult to reconstruct temporal
69 trends of contamination and the origins of these latter from legacy sediments. So, determining
70 the origins of contamination in an estuary requires to study its tributaries.

71 The Seine River watershed (France) provides an example of a basin experiencing
72 anthropogenic activities. The industrial revolution increased the anthropogenic pressure on the
73 Seine River considerably over a period of about 150 years, resulting in specific and drastic
74 changes in the stream morphology. These modifications meant that the flow of the Seine
75 River was regulated, mainly to facilitate navigation in the nineteenth century (Horowitz et al.,
76 1999; Lestel et al., 2019). The morphological modifications also impacted the tributaries of
77 the Seine River. Thus, the Eure River, the most important contributor to the Seine Estuary,
78 saw its outlet diverted 11 km downstream between 1929 and 1939. All these adjustments have

79 promoted the establishment of depositional environments favouring the storage of legacy
80 sediments suitable for reconstructing anthropogenic activities in the watershed. However, if
81 the history of the Seine River is well known, there is less historical information about its
82 tributaries; the latter could potentially be the main source of contamination in the lower
83 reaches of the watershed, i.e., the estuary (e.g. the Gironde Estuary; Audry et al., 2004;
84 Masson et al., 2006). Most sediment cores covering at least the last 70 years were extracted
85 along the Seine Estuary (Van Metre et al., 2008; Vrel, 2012; Vrel et al., 2013; Kaci et al.,
86 2014, 2016) and along the fluvial part of the Seine River, upstream from the Poses Dam
87 (Figure 1A; Bonté et al., 2004; Meybeck et al., 2007; Ayrault et al., 2010a; Le Cloarec et al.,
88 2011; Tamtam et al., 2011; Ayrault et al., 2012; Vrel et al., 2013; Lorgeoux et al., 2016). In
89 contrast, there are few sediment records for the tributaries (Figure 1B; Ayrault et al., 2010b;
90 Le Cloarec et al., 2011; Ayrault et al., 2012). Unfortunately, the geographic locations of the
91 cores from the Oise and Marne rivers restricted the reconstruction of the sedimentary and
92 contamination history to a limited area of these two tributaries. The best location for coring is
93 at the outlet of a tributary, where the geochemical signatures of the river being studied can
94 best be captured.

95 This is the reason that anthropogenic activities in the Eure River watershed were
96 investigated, for the first time, using sediment cores collected from two ponds near the outlet.
97 As recently raised by Bábek et al. (2020), the spatial distribution of sediments in the
98 depositional zones (behind a dam in the case of this study) and thus the spatial distribution of
99 sediment-associated contaminants, is rarely studied. In addition, it is generally accepted that
100 the studied sediment core is representative of the watershed signals, but without the absolute
101 certainty that a local disruption could have disturbed the global recorded signal. Hence, it is
102 difficult to know if the studied sediment core is representative of (i) the whole depositional
103 zones and, (ii) the global signature of the inputs from the whole watershed. To circumvent this
104 uncertainty, sediment cores were collected in our study in two ponds in order to ensure that

105 the recorded sedimentological and geochemical signatures are not disturbed by local inputs
106 and can be considered as representative of the whole watershed. In addition, and for each
107 ponds, the representativeness of the sediment cores was investigated with ground-penetrating
108 radar profiles. Our study also proposes an original coupling between sedimentological and
109 geochemical analyses to assess the deposition conditions and the nature of the sediment
110 deposits as they can influence the temporal trends of trace metal elements TME (Dhivert et
111 al., 2015). Lastly, the morphological changes modifying the depositional conditions have been
112 studied by using historical documentaries as seen in previous studies (Pittam et al., 2009;
113 Grygar et al., 2016).

114 Hence, combining a comprehensive set of geophysical, sedimentological, geochemical
115 methods and, historical documentaries, our main objectives were to (i) determine the
116 consequences of the morphological modifications of depositional zones during the diversion
117 of the Eure River outlet on the sedimentary dynamic, (ii) determine the nature of these legacy
118 sediment deposits and (iii) reconstruct the temporal trends of anthropogenic activities with a
119 focus on TME considered as markers of industrial activities in the Eure River watershed. This
120 study also discussed the reactivity of the watershed to anthropogenic activities, and the
121 resilience of the system to overcome these stresses.

122

123 **2. Material and Methods**

124

125 **2.1. Setting**

126

127 The Seine River flows into the Paris Basin. Sedimentary formations (Jurassic limestone and
128 marls, Cretaceous chalk, carbonaceous alluvial, and Tertiary quartz deposits) cover most of
129 the basin, with carbonate formations dominating (Thibert, 1994). The Eure River watershed

130 (Figure 1B) is underlain by a chalk formation from the Upper Cretaceous, covered by sandy-
131 clay deposits from the Tertiary and Quaternary deposits (Quesnel, 1997; Laignel et al., 1998).
132 The Eure River is the fourth largest tributary of the Seine Basin in terms of area (6 017 km²),
133 and the fifth in terms of flow at the outlet ($Q_{\text{mean}} = 22.1 \pm 6.7 \text{ m}^3 \text{ s}^{-1}$) for the period from 1971
134 to 2019 (www.hydro.eaufrance.fr).

135 Until the end of the nineteenth century, there were numerous islands spread through the
136 channel of the Seine Estuary. At that time, the Eure River outlet was more than 11 km
137 upstream of the present outlet (Figure 2A). Therefore, the studied coring sites at Martot and
138 Les Damps did not exist (see section 2.2) and were in the left branch of the Seine Estuary,
139 which was a dynamic riverine environment, unfavourable to sediment deposition.

140 Between 1861 and 1864, the Martot Dam (needle dam), the first of its scale in the Seine
141 Estuary, was built in two parts (169.6 m + 135.0 m) across two branches of the Seine River
142 (Figure 2B). During the 1880s, the Poses Dam was constructed further upstream (Figure 1A).
143 These two dams were built in a section of the Seine Estuary where navigation was made
144 difficult by the presence of the islands and natural weirs. The first major modification that
145 impacted the Eure River dates back to the 1930s (1929–1935), when the Eure River outlet
146 was moved 2 km downstream by following a former part of the left branch of the Seine River
147 (Figure 2C). This morphological modification formed a pond connected to the Eure River
148 (Les Damps Pond). The entire section was completely disrupted during the 1930s, and the
149 channel of the Seine River was deeply restructured. During this period, the channel
150 morphology of the Seine River was modified, in some cases by passing through former
151 islands or by filling connections between the many islands present in its channel. Between
152 1937 and 1939, the Eure River outlet was moved 9 km downstream by following the former
153 branch of the Seine River and was relocated at the Martot Dam. At the same time, a dike was
154 built in the middle of the Martot Dam in the direction of the flow to isolate a pond (Martot
155 Pond). In 1939, the connection between Martot Pond and the Seine River was filled to

156 calibrate the Seine River channel while a connection between Martot Pond and the Eure River
157 was opened thereafter. The Martot Dam became obsolete when the connections between the
158 islands were filled and was partially removed between 1938 and 1941, leaving only the part
159 across the branch of the Eure River (Figure 2D).

160 The area did not experience further evolution until 2017 when the Martot Dam was removed
161 following the Water Framework Directive (2000/60/CE), to facilitate the continuity of
162 sediment transport.

163

164 2.2. Sampling sites

165

166 2.2.1. *Upstream site: Les Damps Pond*

167 Les Damps Pond (formed between 1929–1935) is upstream of the Eure River spillway
168 (Figure 3A). The pond, which has an average depth of 50 cm and an area of less than 1 ha, is
169 connected to the Eure River, even during low water periods, and continually accumulates
170 suspended particulate matter (SPM) from the Eure River watershed (Figure 3B). Because the
171 site is 2 km upstream of a spillway, the tides have no noticeable effect, even in the case of a
172 high tidal coefficient.

173 The cores were extracted from this pond in January 2015 and 2017, using a gravity corer
174 (UWITEC) and PVC tubes with a diameter of 90 mm. The water-sediment interface was
175 preserved during coring (Table 1).

176

177 2.2.2. *Downstream site: Martot Pond*

178 Cores were also extracted from Martot Pond (area ~ 7 ha), in the lower reaches of the study
179 area (Figure 3A). Martot Pond is affected by the waters of the Seine River during tidal flows
180 through the Eure River outlet. However, the impact of the tide is limited and temporally
181 variable, as its flow persists for about 3 h and does not occur every day, because the dam,

182 located 200 m downstream from the connection with this pond, stops tidal flows for tidal
183 coefficients lower than 70 (until the removal of the dam in 2017) (Figure 3C). Thus, to ensure
184 Martot Pond was not impacted by the Seine River flow, results from this core site were
185 compared with those from Les Damps Pond. The Martot Dam also regulated the water level
186 in the river and the latter was continuously connected to the Martot Pond, even during periods
187 of low flow.

188 The cores were extracted from this pond in January and May 2015 and February 2017, using
189 a gravity corer (UWITEC) and PVC tubes with a diameter of 90 mm. The water-sediment
190 interface was preserved during coring (Table 1).

191

192 2.3. Geophysical investigation: GPR

193

194 Ground penetrating radar (GPR) is a non-invasive geophysical technique that detects
195 electrical discontinuities. It is based on the generation, transmission, propagation, reflection,
196 and reception of discrete pulses of high frequency electromagnetic energy (MHz). For several
197 years, it has been particularly used in the study of sedimentary structures and deposition
198 environments in fluvial environments (Huggenberger et al., 1994; Asprion and Aigner, 1999;
199 Beres et al., 1999; Bristow and Jol, 2003; Neal, 2004; Kostic et al., 2005; Huggenberger and
200 Regli, 2006; Bábek et al., 2008; Słowik, 2015; Gu et al., 2019). In this study, the surveys were
201 carried out in an aquatic environment (Water GPR-WGPR) because it is possible to tow the
202 antennas of the geological radar in or behind a boat (Mellett, 1995; Lin et al., 2009; Sebok et
203 al., 2018). The GSSI SIR 4000 acquisition system (Geophysical Survey System Inc., Salem,
204 USA) was connected to a Trimble GPS with a 400 MHz antenna. The instrumentation was
205 loaded on a high density polyethylene boat. A total of five longitudinal profiles was acquired
206 closest to the sampled cores, at both of the two sites (Figures 3B & 3C). The data were
207 processed with Radan 7 software (GSSI copyright) to obtain interpretable radargrams. A

208 velocity of 0.075 m ns^{-1} was determined using the hyperbola method and the correlation with
209 sediment cores. This is of the same order of magnitude as the measurements made by Lin et
210 al. (2009) (0.076 m ns^{-1}) and O'Driscoll et al. (2010) (0.06 m ns^{-1}) on comparable sediments.

211

212 2.4. Sedimentological analysis

213

214 2.4.1. *Grain size distribution*

215 The grain size distribution can influence the behaviour of chemical compounds. Radioactive
216 tracers (^{210}Pb , ^{137}Cs , and ^{241}Am) are preferentially adsorbed onto fine particles (Livens and
217 Baxter, 1988; Walling and Woodward, 1992; Wang and Cornett, 1993; He and Walling, 1996;
218 Monna et al., 1998; Gil-García et al., 2009) as well as organic and metallic contaminants
219 (Horowitz and Elrick, 1987; Walling et al., 2003; Grosbois et al., 2006; Devault et al., 2009;
220 Coynel et al., 2016). Thus, the grain size distribution can have a considerable impact on
221 radioactive tracers and TME concentrations along sediment cores (He and Walling, 1996).
222 Differences in grain size are also excellent indicators of flood events or anthropogenic
223 activities (e.g. changes in land use) (Kurashige and Fusejima, 1997; Weltje, 2012; Toonen et
224 al., 2015; Collins et al., 2017).

225 The grain size distribution of the sediment cores was measured by laser diffraction (LS
226 13320 Particle Size Analyser Beckman Coulter™). The measurements were realised every cm
227 by integrating 1 cm on the DAM15-02 and MAR15-01 cores.

228

229 2.4.2. *Total organic carbon content*

230 The total organic carbon (TOC) and organic matter (OM) quality can also influence TME
231 concentrations (Audry et al., 2006; Tseng et al., 2001; Masson et al., 2011; Petit et al., 2013;
232 Coynel et al., 2016). Moreover, variations in TOC and related parameters (e.g. HI and OI)
233 provide information on the hydrological dynamics and anthropogenic impact in a watershed.

234 The TOC content was measured using Rock-Eval 6 (RE6) pyrolysis (“Turbo” model RE6
235 pyrolyzer, at the ISTO laboratory, University of Orléans), as described in Copard et al.
236 (2006). The OM quality was obtained from measuring HI (hydrogen index, in mg HC g⁻¹
237 TOC) and OI (oxygen index, in mg O₂ g⁻¹ TOC). HI corresponds to the quantity of HC
238 released relative to TOC, while OI reflects the quantity of oxygen released as CO and CO₂
239 relative to TOC. Used together, these two parameters in the pseudo Van-Krevelen diagram
240 (HI vs OI) can support the identification of the OM origin and its subsequent processes
241 (Tissot and Welte, 1984). These variables were measured on the DAM17-02 (at intervals of 2
242 cm) and MAR15-01 cores (at intervals of 1 cm).

243

244 2.4.3. *Magnetic susceptibility*

245 The magnetic properties of accumulated stored sediments are generally used to identify
246 detrital inputs (e.g. from floods) (Debret et al., 2010) and anthropogenic modifications (e.g.
247 metallic pollution in soils and sediments) (Hanesch and Scholger, 2002; Knab et al., 2006;
248 Magiera et al., 2006; Blaha et al., 2008). The magnetic properties of the sediment can also be
249 used to determine the origin of the particles (Caitcheon, 1998; Hatfield and Maher, 2008,
250 2009; Hatfield and Stoner, 2013; Collins et al., 2017).

251 The magnetic susceptibility (MS) of the cored sediments was measured using a Bartington
252 MS2E point sensor as described in Debret et al. (2010). The MS of the sediment from the
253 DAM15-02, DAM15-03, DAM17-02, MAR15-01, and MAR15-05 cores was determined.

254

255 2.4.4. *Spectrocolorimetry*

256 Various parameters that can be determined using a spectrophotometer, such as reflectance
257 (L*) and the first derivative reflectance spectra (FDS), may be used to determine the nature
258 and the origin of sediment deposits, and sediment dynamics (Debret et al., 2006, 2011; Sebag
259 et al., 2013). L* describes the lightness of the sediment without any information on the nature

260 of the sediment. FDS provides qualitative information about the major components (such as
261 clay and carbonates) of the sediment deposits. The Q7/4 diagram (700 nm/400 nm ratio vs
262 L*) proposed by Debret et al. (2011) is used to determine the sedimentary dynamics.

263 A Konica Minolta CM 2600d was used to measure the intensity of the reflectance of the
264 sediment in the visible domain (360–740 nm with a spacing of 10 nm) as described in Debret
265 et al. (2011).

266 These measurements were obtained for the DAM15-02, DAM15-03, DAM17-02, MAR15-
267 01, MAR15-02, MAR15-03, MAR15-04, MAR15-05, and MAR16-02 cores.

268

269 2.5. Geochemical analysis by XRF core scanning (XRF-CS)

270

271 X-Ray fluorescence spectrometry (XRF) is used to determine the major and trace element
272 composition of sediment deposits (Richter et al., 2006). The XRF core scanning data can be
273 used to describe particular TME contamination in sediment cores (Battiston et al., 1989;
274 Dickinson et al., 1996; Lepland et al., 2010; Sabatier et al., 2014; Guédron et al., 2016;
275 Hennekam et al., 2019). The data presented were normalised by Ti (considered as a better
276 “normalising element” than Al) to remove possible variations because of detrital inputs
277 (Kylander et al., 2011; Duan et al., 2014; Bábek et al., 2015; Chawchai et al., 2016).

278 The relative contents of the major and trace elements were measured using an XRF
279 Avaatech core scanner (EDYTEM, University of Savoie Mont Blanc). An X-Ray beam was
280 generated with a rhodium anode and a 125 µm beryllium window, which allows a voltage
281 range from 7 to 50 kV and a current range of 0 to 2 mA. The analytical settings were adjusted
282 at 10 kV and 1 mA to detect light elements, and trace elements (namely Pb, Cu, Zn, and Ni)
283 were detected in a second run, performed at 30 kV for 0.75 mA. Each individual power
284 spectrum was transformed by deconvolution into its relative contents (intensities), expressed

285 in counts per second (cps). Measurements were realised every 5 mm for the MAR15-01 and
286 DAM17-02 cores and every 2 mm for the MAR16-02 and DAM15-02 cores.

287

288 2.6. TME analysis

289

290 Microwave-assisted sediment digestion for particulate trace metal analysis (Pb, Zn, Cu,
291 presented in this study) was performed on samples collected in the MAR16-02 core (0.5 g of
292 dry, powdered and homogenised sediment) with aqua regia (HNO₃: 3 mL TraceMetal™
293 Grade; HCl: 9 mL TraceMetal™ Grade). Following the mineralisation, the solutions were
294 diluted in 100 ml of Milli-Q® water. Particulate trace metal concentrations were measured by
295 inductively-coupled-plasma atomic emission spectroscopy (ICP-AES) (iCAP 6000 Series,
296 Thermo Fischer®) performed with external calibration. The accuracy and precision of the
297 measurements were checked against a certified reference material (Trace Element on Fresh
298 Water Sediment CNS301-04-050, Sigma Aldrich) and the results showed accuracies of ≥ 98
299 % with a precision of ≤ 4 % (RSD). All of the analyses were carried out in triplicate (standard
300 deviation ≤ 1.1 %).

301

302 2.7. Short-lived radionuclides

303

304 The activities of ²¹⁰Pb in excess (²¹⁰Pb_{ex}), ¹³⁷Cs, and ²⁴¹Am were determined on samples
305 from the MAR15-01 core (at steps of 1, 4, or 6 cm) using a germanium spectrometer with
306 ultra-low background noise at the Laboratoire Souterrain de Modane (LSM). The age model
307 was computed with the *serac* R package (<https://github.com/rosalieb/serac>, (Bruel and
308 Sabatier, Submitted).

309

310 3. Results

311

312 3.1. Sedimentological characterisation of the sediment cores

313

314 3.1.1. *Les Damps Pond*

315 The sediment cores all showed similar sedimentary facies called U1 (Figures 4A1 & 4A2).

316 The grain size distribution was homogeneous (median (D_{50}) = $29.5 \pm 6.7 \mu\text{m}$) and showed

317 only one population, centred around the D_{50} . (Figure 4B). The TOC content was high and

318 constant ($\text{TOC}_{\text{mean}} = 5.36 \pm 0.47 \%$). HI and OI were also constant, and the values of HI were

319 higher than those of OI ($\text{HI}_{\text{mean}} = 302 \pm 23 \text{ mg HC g}^{-1} \text{ TOC}$ and $\text{OI}_{\text{mean}} = 145 \pm 10 \text{ mg O}_2 \text{ g}^{-1}$

320 TOC) (Figure 4C).

321 The MS values were high and constant between 60 and 90 cm ($\text{MS}_{\text{mean}} = 12 \pm 2$) but had a

322 peak at 50–60 cm. The values decreased between 50 and 30 cm and were constant above 30

323 cm ($\text{MS}_{\text{mean}} = 6 \pm 1$) (Figure 4D).

324 The values of L^* were low and constant ($L^*_{\text{mean}} = 28.5 \pm 2.3 \%$), with values between 22

325 and 38 % (Figure 4D).

326 The intensities of FDS were high at wavelengths between 675 and 735 nm. This signature

327 was continuous, and the intensity did not vary, which may mean that the origin of the

328 sedimentary inputs remained the same throughout the sedimentation (Figure 4E).

329 The Pb/Ti ratio was low and constant ($\text{Pb/Ti}_{\text{mean}} = 0.64 \pm 0.12$) between 30 and 80 cm but

330 increased at 30 cm. The values of the ratio were generally high between 0 and 30 cm

331 ($\text{Pb/Ti}_{\text{mean}} = 2.26 \pm 0.58$) and decreased from 15 cm to the surface (Figure 4F). The Zn/Ti,

332 Cu/Ti, and Ni/Ti ratios showed the same trend. These three ratios were high between 30 and

333 80 cm and reached maximum values between 50 and 60 cm ($\text{Zn/Ti}_{\text{mean}} = 2.04 \pm 0.24$,

334 $\text{Cu/Ti}_{\text{mean}} = 1.43 \pm 0.71$, and $\text{Ni/Ti}_{\text{mean}} = 0.04 \pm 0.01$). Around 30 cm, the ratios decreased and

335 were constant between 0 and 30 cm (Figure 4F).

336

337 3.1.2. Martot Pond

338 The sediment cores showed two sedimentary facies delimited by a transition zone at 75–80
339 cm. In this section, the results from the MAR15-01 core are presented. The upper facies (0–75
340 cm) is referred to as U1, while the lower facies (75–138 cm) is referred to as U2 (Figure 5A).

341 • U2 facies:

342 The grain size distribution was homogeneous (median (D_{50}) = $13.8 \pm 7.0 \mu\text{m}$) and showed
343 one population centred around D_{50} (Figure 5B). The TOC content was low and constant
344 ($\text{TOC}_{\text{mean}} = 1.75 \pm 0.33 \%$). HI was constant ($\text{HI}_{\text{mean}} = 147 \pm 24 \text{ mg HC g}^{-1} \text{ TOC}$) and lower
345 than OI ($\text{OI}_{\text{mean}} = 260 \pm 35 \text{ mg O}_2 \text{ g}^{-1} \text{ TOC}$). OI increased, peaked at 103.5 cm ($\text{OI} = 347 \text{ mg}$
346 $\text{O}_2 \text{ g}^{-1} \text{ TOC}$), then decreased. The only exception to this trend was at the depth of 128.5 cm
347 (Figure 5C).

348 The MS was low and L^* was high and constant ($L^*_{\text{mean}} = 44.4 \pm 2.1 \%$), with values
349 between 40 and 50 % (Figure 5D).

350 The intensities of FDS were high for wavelengths between 365 and 550 nm. A second
351 signature, less intense, was also visible for high wavelengths (675–735 nm). This indicates
352 that several signatures were marked within the facies and the small variations in intensity
353 suggest the origin of the whole U2 facies was unique (Figure 4E).

354 The Pb/Ti, Zn/Ti, Cu/Ti, and Ni/Ti ratios were low and constant ($\text{Pb/Ti}_{\text{mean}} = 0.33 \pm 0.10$,
355 $\text{Zn/Ti}_{\text{mean}} = 0.54 \pm 0.11$, $\text{Cu/Ti}_{\text{mean}} = 0.18 \pm 0.05$, and $\text{Ni/Ti}_{\text{mean}} = 0.04 \pm 0.01$) and were higher
356 only at the transition between the two facies in the 75–80 cm depth interval (Figure 5F).

357 • U1 facies:

358 The grain size distribution was homogeneous (median (D_{50}) = $33.9 \pm 7.8 \mu\text{m}$) and had one
359 population centred around D_{50} (Figure 5B) as in Les Damps Pond. The TOC content was
360 twice as high in U1 ($\text{TOC}_{\text{mean}} = 3.88 \pm 1.49 \%$) as in U2, and the values were particularly high

361 near the top of the core (TOC = 8.26 ± 0.19 % between 9 and 12 cm). HI increased upwards
362 from the transition between U1 and U2 and stabilised at a depth of 66.5 cm. OI continued to
363 decrease in U1 and stabilised at a depth of 66.5 cm in U1. At the opposite end of the U2
364 facies, HI was high ($HI_{\text{mean}} = 279 \pm 23$ mg HC g⁻¹ TOC) and OI was low ($OI_{\text{mean}} = 150 \pm 17$
365 mg O₂ g⁻¹ TOC) (Figure 5C) as described along the U1 facies in Les Damps Pond.

366 The U1/U2 transition was marked by a strong increase in MS and a decrease in L*. The MS
367 values were high ($MS_{\text{mean}} = 25 \pm 7$) from 45 to 75 cm but were lower ($MS_{\text{mean}} = 8 \pm 4$)
368 between 0 and 45 cm (Figure 5D). The L* was lower in the U1 facies ($L^*_{\text{mean}} = 34.1 \pm 4.2$ %)
369 than in the U2 facies, and was almost the same as the values between 24 and 40, and
370 decreased next to the top of the core (Figure 5D). The sediment colour was similar to that in
371 the U1 facies in Les Damps Pond.

372 The intensities of FDS were high at high wavelengths (675–735 nm), but, unlike the U2
373 facies, low wavelength signatures were not noticeable. This indicates a major change in the
374 nature of the sediment stored in Martot Pond (Figure 5E). Moreover, the signature was
375 continuous and the intensity did not vary as in Les Damps Pond.

376 The Pb/Ti ratio increased at the U1/U2 transition but remained stable to a depth of 35 cm
377 ($Pb/Ti_{\text{mean}} = 1.06 \pm 0.15$ between 35 and 75 cm). The ratio was higher from 35 to 10 cm
378 ($Pb/Ti_{\text{mean}} = 3.17 \pm 0.53$ between 10 and 35 cm) and trended to decrease closer to the top of
379 the core (Figure 5F). The patterns in the Zn/Ti, Cu/Ti, and Ni/Ti ratios were similar. Indeed,
380 from the transition between U1 and U2, the ratios increased and peaked between 50 and 60
381 cm ($Zn/Ti_{\text{mean}} = 4.79 \pm 0.73$, $Cu/Ti_{\text{mean}} = 1.19 \pm 0.20$, and $Ni/Ti_{\text{mean}} = 0.11 \pm 0.01$). The ratios
382 decreased from 50 to 35 cm and then stabilised above 35 cm (Figure 5F). The variations in the
383 Pb/Ti, Zn/Ti, Cu/Ti, and Ni/Ti ratios generally followed a similar pattern to those described
384 for Les Damps Pond.

385

386 3.2. TME concentrations along the U1 facies in Martot Pond

387

388 The trends in the Pb/Ti, Zn/Ti, and Cu/Ti ratios for the top 77 cm of the MAR16-02 core
389 and the U1 facies of the MAR15-01 core were similar, which shows that this facies was also
390 well represented within MAR16-02. The Pb, Zn, and Cu concentrations were measured at the
391 depths for which the XRF ratios reached maximum and minimum values within the MAR16-
392 02 core (Figure 6).

393 The Pb concentration was constant to a depth of 35 cm ($Pb_{\text{mean}} = 120 \pm 28 \text{ mg kg}^{-1}$), apart
394 from at 65 cm ($Pb = 190 \text{ mg kg}^{-1}$). The Pb concentrations increased in the same way as the
395 Pb/Ti ratio, and the concentrations were highest at 12 cm ($Pb = 669 \text{ mg kg}^{-1}$). Near the top of
396 the core (4 cm), the Pb concentration decreased, similar to the Pb/Ti ratio, and at 299 mg kg^{-1}
397 it was less than half the maximum concentration at 12 cm but almost 2.5 times the average
398 concentration below 35 cm (Figure 6). The Zn and Cu concentrations were 415 mg kg^{-1} and
399 113 mg kg^{-1} at 77 cm, respectively. The concentrations of these two TMEs peaked at 65 cm
400 ($Zn = 905 \text{ mg kg}^{-1}$, $Cu = 399 \text{ mg kg}^{-1}$). Between 10 and 40 cm, the Zn and Cu concentrations
401 were less than half and less than a quarter of the maximum concentrations, respectively, and
402 the Zn/Ti and Cu/Ti ratios were also low close to the top of the MAR16-02 core (Figure 6).
403 The Zn and Cu concentrations at 4 cm were lower than those measured at 77 cm.

404

405 3.3. Age model of the MAR15-01 core

406

407 Recent deposit dating and sedimentation rate estimates have been realised from short-life
408 radionuclides (Robbins and Edgington, 1975; Appleby and Oldfield, 1978; Appleby et al.,
409 1991; He and Walling, 1996; Mabit et al., 2014). The sedimentation rate was determined from
410 the $^{210}\text{Pb}_{\text{ex}}$ by subtracting the ^{226}Ra activity from the $^{210}\text{Pb}_{\text{total}}$ (Krishnaswamy et al., 1971).
411 The ^{137}Cs and ^{241}Am activities were used to identify nuclear weapon testing with maximum

412 activity in 1963, and the Chernobyl accident in 1986 and are used to confirm the age model
413 established with $^{10}\text{Pb}_{\text{ex}}$.

414 The activity of $^{210}\text{Pb}_{\text{ex}}$ was measured to 80 cm and decreased almost continuously with
415 depth. A sedimentation rate of 12.73 mm y^{-1} ($R^2 = 0.60$) was estimated using the ‘constant
416 flux, constant sedimentation rate’ (CFCS) model (Krishnaswamy et al., 1971) (Figure 7A).
417 The ^{137}Cs and ^{241}Am activities peaked at 60 and 58 cm, respectively, corresponding to the
418 maximum fallout from atmospheric nuclear weapon testing in 1963 (Robbins and Edgington,
419 1975; Appleby et al., 1991) (Figure 7B). There was also a peak in the ^{137}Cs activity at 40 cm,
420 perhaps related to the Chernobyl accident in 1986 (Figure 7B). An age model was realised for
421 the U1 facies of the MAR15-01 core using the sedimentation rate obtained from the $^{10}\text{Pb}_{\text{ex}}$
422 (Figure 7C).

423

424 **4. Discussion**

425

426 4.1. Sedimentary filling in the depositional zones

427

428 As the sedimentological parameters are presented for one core from Martot Pond (two cores
429 in the case of Les Damps Pond), it is essential to ensure that the studied cores are
430 representative of sediment records in the entire respective pond. Concerning Martot Pond, a
431 sediment thickness between 2.0–2.5 m is showed by the radargram GPR_MAR_08 (Figure
432 8A). The reflector R1 made it possible to distinguish two islands without a well-differentiated
433 structure on this scale, which may correspond to parts of the central island that separated the
434 two branches of the Seine River (Figure 2). A second reflector (R2, solid red line) between
435 350 m and 550 m separates U1 and U2 and this interpretation is justified by the MAR15-02
436 core in which this limit is observed at 85 cm (corresponding to the transition between U1 and
437 U2 observed on MAR15-01 core at 75–80 cm). Beyond this section, it is more difficult to

438 locate R2, but the position of the MAR15-03, MAR15-04 and MAR15-06 cores, with the aid
439 of some clues, allowed us to position R2 (red dotted line). Geophysical prospecting shows a
440 homogeneous filling within Martot Pond and thus validates the representativeness of the
441 studied core.

442 Concerning Les Damps Pond, two quality profiles have been obtained (Figures 8B & 8C) in
443 which a reflector (R3) showed the lower limit of U1. In this facies, few continuous structures
444 were detectable, probably because of the fine accumulated sediments and the monotony of the
445 sediment as observed in the DAM15-02 and DAM17-02 cores. However, under R3, it was
446 possible to distinguish less powerful reflectors, probably attributed to the presence of a bed of
447 coarser material (Figure 8B). This reflector was therefore interpreted as the upper limit of the
448 former stream-bed of the Seine River. Hence, the two studied sediment cores are
449 representative of the sedimentary records of the entire pond.

450

451 4.2. Identification of the deposition conditions and sediment origin

452

453 The grain size in the U2 facies ($D_{50} = 13.8 \pm 7.0 \mu\text{m}$) of Martot Pond and in the U1 facies of
454 Martot and Les Damps Ponds ($D_{50} \sim 30 \mu\text{m}$) suggests a weak sedimentation dynamic, that is,
455 deposition under very low flow conditions, but also suggests two distinct unidentified origins.
456 U2 was also characterised by an HI/OI ratio < 1 (Figure 9A), reflecting the input of material
457 from a terrestrial origin (Carrie et al., 2012). In detail, the values of these two indicators of
458 OM quality reflect an organo-mineral soil horizons origin (A horizon) (Disnar et al., 2003).
459 Conversely, the U1 facies of both ponds are characterised by an HI/OI ratio of approximately
460 2 (Figure 9A), suggesting that the OM origin is either aquatic (Carrie et al., 2012) or, with
461 respect to the HI and OI values, detrital (OH or A horizons) (Disnar et al., 2003). Therefore,
462 OM in the U1 facies is less altered and may have a mix aquatic/terrestrial origin, than that
463 stored in the U2 facies.

464 Spectrocolorimetry data for U2 showed a sedimentary dynamic mainly structured around
465 two end-members which are poles “clayey deposits” and “carbonate deposits” (Figure 9B).
466 The clayey deposits pole reflects the input of detrital clay sediments while the carbonate
467 deposits pole reflects the input of light sediments because of their carbonate contents. These
468 results were confirmed by FDS and show a predominance of the carbonate signature (Debret
469 et al., 2011). The U2 facies is therefore the consequence of the sedimentation of a clay-
470 carbonate material, with an organic component that had a terrestrial origin. This terrigenous
471 deposit, which accumulated in a low intensity zone, may be derived from the erosion of the
472 carbonate substratum of the Seine River watershed.

473 In terms of the U1 facies of both ponds, there was sedimentation consisting of fine
474 sediments enriched in OM. Indeed, the U1 facies is close to the poles of “clayey deposits” and
475 “organic-rich sediment (*Chlorophyll-a* and *by-products*)” (Figure 9B). This organic pole, also
476 confirmed by the FDS (Debret et al., 2011), could be explained by high aquatic primary
477 production and also by a less degraded soil OM. Such mixing is also verified by the pseudo
478 Van-Krevelen diagram.

479 The similar trend of the U1 facies from the two ponds, and the absence of a clear depth
480 distribution in the pseudo Van-Krevelen and Q7/4 diagrams (Figure 9), suggest that (i) SPM
481 are not altered by any processes between the ~10 km separating the two ponds and, (ii)
482 sediment deposits were not submitted to post-depositional alterations (e.g., early diagenesis),
483 probably due to a high sedimentation rate (Van Metre et al., 1997; Horowitz et al., 1988;
484 Callender and Robbins, 1993; Callender, 2000; Audry et al., 2004). Hence, there is a common
485 origin of sediments from both U1 facies, corresponding to the inputs from the Eure River (U1
486 = Eure Unit) and consequently, intrusions of the Seine River into Martot Pond (during tidal
487 flow) do not alter the Eure River signature. Therefore, the U1 facies from Martot Pond was
488 considered as representative of the Eure River signal recorded in sediments, and so was used
489 to build an age model.

490

491 4.3. Links with the morphological modification of the Seine and Eure Rivers

492

493 According to the age model established for the MAR15-01 core, the transition between the
494 U2 facies and the Eure Unit date from around 1954 ± 10 y. The history of the study site
495 showed that Martot Pond was disconnected from the Seine River from 1939. The recently
496 shaped connection between Martot Pond and the Eure River seems consistent with this
497 change, or else dated from the early 1940s. The age model therefore seems consistent with the
498 morphological modification, and the facies change was established at 1939–1944, when
499 Martot Pond was isolated from the Seine River.

500 The U2 facies was deposited before this major change. The history of the study site shows
501 that, before the Eure River outlet was diverted, the present Martot Pond corresponded to the
502 area behind the Martot Dam, supplied by waters from the Seine River. The U2 facies
503 corresponds to sedimentation of material from the Seine River watershed upstream of the
504 dam. Moreover, the GPR prospecting showed that, in some places, the potential lower limit of
505 this unit corresponded to parts of the island separating the two branches of the Seine River.

506 The sediment stored in Martot Pond would be useful to study the Eure River basin from the
507 early 1940s. However, the lack of dating means that, to date, the U2 facies (Seine Unit) has
508 not been analysed in detail and will be the subject of a future prospectation.

509

510 4.4. Identification of an anthropogenic imprint in the Eure River facies

511

512 According to the correlation matrix, the major elements (Si, Fe, Al, and Ti) were strongly
513 correlated with each other ($0.69 < R < 0.87$) (Figure S1). The input of these major elements
514 represents the detrital inputs from the Eure River watershed. The trace elements (Zn, Cu, Ni,
515 and Pb) were not correlated with major elements, demonstrating that their presence within the

516 Eure Unit was not linked to the natural input of the Eure River watershed. In addition, Zn, Cu,
517 and Ni were positively correlated with each other ($0.79 < R < 0.88$), indicating a common
518 source in the watershed (Figure S1). The lack of correlation between TME and fine particles,
519 as well as the homogeneity of the grain size distribution, indicates that the TME variations
520 were related to anthropogenic contributions rather than lithological variations. This lack is
521 also seen with the OM, because the variation in TOC vs TME is not correlated. Lastly, the
522 sedimentation rate does not control the TME variations, as the latter was estimated as constant
523 over the considered period.

524 As a consequence, the temporal variations in the semi-quantitative Zn, Cu, Ni, and Pb data
525 were related to changes in the input of particulate TME. These variations may reflect the
526 presence of new sources within the watershed, and may be related to anthropogenic activities
527 that occurred during the second half of the twentieth century.

528

529 4.5. Reconstruction of Pb history

530

531 In large European watersheds, Pb levels generally exhibit similar temporal trends with
532 increases from the 1940s until the 1970s, then decreases until the 1990s (Danube and Rhine
533 Rivers : Winkels et al., 1998; Loire River : Grosbois et al., 2006; Seine River : Le Cloarec et
534 al., 2011; Ayrault et al., 2012; Rhône River : Ferrand et al., 2012). Conversely, in the Eure
535 River, Pb levels were stable during the 1960s, increased at the end of the 1980s, and reached a
536 maximum in the 1990s and 2000s followed by a decrease after 2006 (Figure 10). The high
537 Pb/Ti ratio values in Martot Pond in the 1990s and 2000s reflect the high Pb concentrations
538 measured along the MAR16-02 core. This high concentration was also seen in SPM and
539 dissolved load collected in the lower reaches of Eure River from March and September 2009
540 (Chiffolleau et al., 2012). In detail, the concentrations were 4–5 times (for particulate
541 concentrations: $Pb_p = 430$ and 380 mg kg^{-1} ; measured on SPM) and 5–10 times (for dissolved

542 concentrations: $Pb_d = 1400 \text{ ng L}^{-1}$ and 800 ng L^{-1}) higher than those measured in the Seine
543 River at Poses and during the same period. Chiffolleau et al. (2012) hypothesised that the high
544 Pb levels were not related to atmospheric input but rather to a cathode-ray tube (CRT) factory
545 containing 1 to 3 kg of Pb (Tsydenova and Bengtsson, 2011) in their leaded glass (Singh et
546 al., 2016). The CRT factory started operating at Dreux in 1956 and a second factory,
547 specialising in the assembly of CRT TVs and the manufacture of electrical circuits, opened in
548 1974 in the same industrial site. The Pb content in the sediments showed little evidence of the
549 successive commencement of these two factories (Figure 10). The industrial production
550 increased from 1990 to the 2000s, when the factories were taken over by the Philips Group,
551 increasing the Pb discharge from the site. To illustrate our statement, the European
552 Environment Agency reported a direct release of 3540 kg of Pb into the water in 2001,
553 exposing it as one of the highest European Pb emitters. Between 2002 and 2005, production
554 decreased, as did Pb release (1900 to 1500 kg of Pb into the water in the years 2003 and 2004)
555 (“IREP,” n.d.). At the commencement of industrial growth, the Pb/Ti ratio began to increase,
556 and reflecting the instantaneous reactivity of the watershed to this anthropogenic disturbance.
557 However, the fall in industrial output did not produce a decrease in the Pb/Ti ratio, which
558 continued to rise into the late 2000s when the industrial sites were definitively closed (Figure
559 10). Again, this signifies that the watershed reacts to anthropogenic changes, however, the
560 decrease in the ratio is slower than initially expected and remains high after the termination of
561 industrial activity. As an example, near the top of the core, the Pb concentration is twice as
562 high as than the average concentration estimated before 1990. As the levels of the Pb/Ti ratio
563 and the Pb concentrations before industrial activity increased (1990s) may correspond to
564 a reference level of Pb concentration in the Eure River, an additional Pb source is expected in
565 the Eure River watershed. Without any other anthropogenic Pb emitters, it is reasonable to
566 conjecture that this is likely related to Pb contaminated soil surrounding the factory and Pb
567 contaminated sediments stored in the riverbanks and channel, which fed Pb into the river

568 during erosion processes. Hence, the watershed was not able to react immediately to the cease
569 of industrial activity, and a resilience period of the system could be identified (Holling, 1973;
570 Folke et al., 2002). In this case, and due to the erosion of contaminated soil and sediments
571 further realising Pb into the environment, it will be take several years or decades for the river
572 to reach the reference level in Pb concentration. The close relationship between this industrial
573 activity and the observed temporal trends in Pb content suggests that this activity is the main
574 source of contamination but does not allow to state that it is the only one.

575

576 4.6. Reconstruction of Zn, Cu, and Ni

577

578 First, the sharp increase in Zn, Cu, and Ni at the transition between the Seine and the Eure
579 Units shows how the modification of the Seine River channel (for navigation) instantly
580 impacted the quality of the sediments deposited in Martot Pond. The historical trends of Zn,
581 Cu, and Ni, reported by several studies in large European rivers, such as the Danube, Rhine,
582 Loire and Seine basins, show that the concentrations increased between 1940 and the 1970s,
583 then decreased (Winkels et al., 1998; Grosbois et al., 2006; Le Cloarec et al., 2011). Just as in
584 these watersheds, the Zn, Cu, and Ni contents in the Eure River watershed were high until the
585 1980s and peaked during the 1960s and 1970s (Figure 10). The strong correlations between
586 these elements suggest a single source to the Eure River, that started before the facies
587 transition, with the Wonder battery factory the likely source. This factory near the Eure River
588 (20 km upstream from Les Damps) manufactured saline batteries (from Zn) and supplied
589 nearly 40 % of the national market in 1966. The history of this industrial activity indicates
590 that in 1971, the factory was the subject of an increased administrative survey by a national
591 agency, prompting reduced discharge into the Eure River (Agence Financière de Bassin
592 “Seine-Normandie,” 1971). This survey is recorded in the sedimentary archive and
593 corresponds to the beginning of the decrease in Cu (Figure 10). Due to a global evolution of

594 the industry (relocation, change in type of batteries), this industry declined in the late 1960s,
595 which is reflected in the Zn, Cu, and Ni contents in the sediments. After the termination of
596 industrial activity (1994), the Zn, Cu, and Ni content remains stable. Here, the watershed
597 seemed to react instantly with the change in anthropogenic activity. Even if we had no
598 historical and industrial arguments to state that this industrial site was the single source of
599 TME in the river, we would suggest that it was the main one, which is supported by the close
600 relationship between its activity and the observed trends in Zn, Cu, and Ni content in the
601 studied core.

602 The stability of the ratios may indicate that TME release has ceased, but this has to be
603 monitored as there is no record of the TME concentrations before the factory opened in 1938
604 (Guermond, 1981). Hence, it is therefore impossible to confirm whether the pre-
605 contamination levels have been restored or whether contaminants are still being released, even
606 at lower levels, as was the case for Pb.

607

608 **5. Conclusion**

609

610 The modification of the Seine River morphology since the nineteenth century has generated
611 depositional zones in the lower Eure River. The transition between the Seine River and the
612 Eure River units was the marker of one of the last main morphological changes undertaken in
613 the Seine River Estuary.

614 A geophysical investigation of both ponds showed a homogeneous filling validating the
615 representativeness of the studied sediment cores. Consequently, our results revealed a regional
616 signature and are not linked to some local conditions.

617 The sedimentary dynamic during deposition and the nature of the sediment were determined
618 to ensure that the TME evolution over time was related to anthropogenic activities.

619 The study of legacy sediments allowed the reconstruction of the industrial trajectory of the
620 watershed since the 1940s. Our results suggested that the Eure River watershed was submitted
621 to high human pressures that could have affected the Seine Estuary.

622 We have demonstrated that the watershed is very sensitive to any disturbance though a
623 resilience period occurs that extends beyond the period of these disturbances, due to erosion
624 of contaminated soil and sediment.

625 In the course of the Anthropocene, sedimentation zones containing contaminated sediments
626 may be impacted by extreme events (e.g. floods) or modified by human activities (e.g. dam
627 destruction, dredging, and channelisation), which may cause a resuspension of these
628 sediments within rivers, constituting a new source of contamination. Such complex processes
629 concern most worldwide rivers, and for the foreseeable future, it will become necessary to
630 determine their own resilience periods.

631

632 **Acknowledgements**

633 This project (OSS 276) was financially supported by the Seine-Normandie Water Agency and
634 the Region Normandie.

635 Authors thank “Voie Navigable de France” and the “Batellerie” Museum for the access to
636 their historical maps and documents.

637

638 **References**

639

- 640 Agence Financière de Bassin “Seine-Normandie,” 1971. Délibération n°71-16 du 21 Octobre
641 1971 désignant les entreprises industrielles soumises à la mesure pour le calcul de leur
642 redevance pollution.
- 643 Appleby, P.G., Oldfield, F., 1978. The calculation of lead-210 dates assuming a constant rate
644 of supply of unsupported ^{210}Pb to the sediment. *CATENA* 5, 1–8.
645 [https://doi.org/10.1016/S0341-8162\(78\)80002-2](https://doi.org/10.1016/S0341-8162(78)80002-2)
- 646 Appleby, P.G., Richardson, N., Nolan, P.J., 1991. ^{241}Am dating of lake sediments.
647 *Hydrobiologia* 214, 35–42. <https://doi.org/10.1007/BF00050929>

648 Ashley, J.T.F., Bushaw-Newton, K., Wilhelm, M., Boettner, A., Drames, G., Velinsky, D.J.,
649 2006. The Effects of Small Dam Removal on the Distribution of Sedimentary
650 Contaminants. *Environ. Monit. Assess.* 114, 287–312. [https://doi.org/10.1007/s10661-](https://doi.org/10.1007/s10661-006-4781-3)
651 006-4781-3

652 Asprion, U., Aigner, T., 1999. Towards realistic aquifer models: three-dimensional georadar
653 surveys of Quaternary gravel deltas (Singen Basin, SW Germany). *Sediment. Geol.*
654 129, 281–297. [https://doi.org/10.1016/S0037-0738\(99\)00068-8](https://doi.org/10.1016/S0037-0738(99)00068-8)

655 Audry, S., Blanc, G., Schäfer, J., Chaillou, G., Robert, S., 2006. Early diagenesis of trace
656 metals (Cd, Cu, Co, Ni, U, Mo, and V) in the freshwater reaches of a macrotidal
657 estuary. *Geochim. Cosmochim. Acta* 70, 2264–2282.
658 <https://doi.org/10.1016/j.gca.2006.02.001>

659 Audry, S., Schäfer, J., Blanc, G., Jouanneau, J.-M., 2004. Fifty-year sedimentary record of
660 heavy metal pollution (Cd, Zn, Cu, Pb) in the Lot River reservoirs (France). *Environ.*
661 *Pollut.* 132, 413–426. <https://doi.org/10.1016/j.envpol.2004.05.025>

662 Ayrault, S., Lorgeoux, C., Moilleron, R., Lherm, D., Tassin, B., Bonté, P., Roy-Barman, M.,
663 Le, M.-F., Lefèvre, I., Priadi, C., Evrard, O., Bordier, L., Mouchel, J.-M., Eurin, J.,
664 Tamtam, F., Dinh, T., Boust, D., Vrel, A., 2010b. Archives sédimentaires, empreintes
665 des micropolluants sur le bassin de la Seine sur 80 ans. *PIREN-Seine Rapp. Act.* 2010
666 34.

667 Ayrault, S., Priadi, C.R., Evrard, O., Lefèvre, I., Bonté, P., 2010a. Silver and thallium
668 historical trends in the Seine River basin. *J. Environ. Monit.* 12, 2177–2185.
669 <https://doi.org/10.1039/C0EM00153H>

670 Ayrault, S., Roy-Barman, M., Le Cloarec, M.-F., Priadi, C.R., Bonté, P., Göpel, C., 2012.
671 Lead contamination of the Seine River, France: Geochemical implications of a
672 historical perspective. *Chemosphere* 87, 902–910.
673 <https://doi.org/10.1016/j.chemosphere.2012.01.043>

674 Bábek, O., Grygar, T.M., Faměra, M., Hron, K., Nováková, T., Sedláček, J., 2015.
675 Geochemical background in polluted river sediments: How to separate the effects of
676 sediment provenance and grain size with statistical rigour? *CATENA* 135, 240–253.
677 <https://doi.org/10.1016/j.catena.2015.07.003>

678 Bábek, O., Hilscherová, K., Nehyba, S., Zeman, J., Famera, M., Francu, J., Holoubek, I.,
679 Machát, J., Klánová, J., 2008. Contamination history of suspended river sediments
680 accumulated in oxbow lakes over the last 25 years. *J. Soils Sediments* 8, 165–176.
681 <https://doi.org/10.1007/s11368-008-0002-8>

682 Bábek, O., Kielar, O., Lendáková, Z., Mandlíková, K., Sedláček, J., Tolaszová, J., 2020.
683 Reservoir deltas and their role in pollutant distribution in valley-type dam reservoirs:
684 Les Království Dam, Elbe River, Czech Republic. *CATENA* 184, 104251.
685 <https://doi.org/10.1016/j.catena.2019.104251>

686 Battiston, G.A., Degetto, S., Gerbasi, R., Sbrignadello, G., 1989. Determination of sediment
687 composition and chronology as a tool for environmental impact investigations. *Mar.*
688 *Chem.* 26, 91–100. [https://doi.org/10.1016/0304-4203\(89\)90054-6](https://doi.org/10.1016/0304-4203(89)90054-6)

689 Bednarek, A.T., 2001. Undamming Rivers: A Review of the Ecological Impacts of Dam
690 Removal. *Environ. Manage.* 27, 803–814. <https://doi.org/10.1007/s002670010189>

691 Beres, M., Huggenberger, P., Green, A.G., Horstmeyer, H., 1999. Using two- and three-
692 dimensional georadar methods to characterize glaciofluvial architecture. *Sediment.*
693 *Geol.* 129, 1–24. [https://doi.org/10.1016/S0037-0738\(99\)00053-6](https://doi.org/10.1016/S0037-0738(99)00053-6)

694 Blaha, U., Appel, E., Stanjek, H., 2008. Determination of anthropogenic boundary depth in
695 industrially polluted soil and semi-quantification of heavy metal loads using magnetic
696 susceptibility. *Environ. Pollut.* 156, 278–289.
697 <https://doi.org/10.1016/j.envpol.2008.02.013>

698 Bonté, P., Cloarec, M.-F.L., Sornein, M.-O., Lefèvre, I., Desalle, T., Mouchel, J.-M., Ayrault,
699 S., 2004. Enregistrement sédimentaire de la contamination métallique, Piren-Seine,
700 Rapport d'activité 2003.

701 Bristow, C.S., Jol, H.M., 2003. An introduction to ground penetrating radar (GPR) in
702 sediments. *Geol. Soc. Lond. Spec. Publ.* 211, 1–7.

703 Bruel, R., Sabatier, P., Submitted. serac : a R package for ShortlivEd RADionuclide
704 Chronology of recent sediment cores. *Quat. Geochronol.*

705 Caitcheon, G.G., 1998. The significance of various sediment magnetic mineral fractions for
706 tracing sediment sources in Killimicat Creek. *CATENA* 32, 131–142.
707 [https://doi.org/10.1016/S0341-8162\(97\)00057-X](https://doi.org/10.1016/S0341-8162(97)00057-X)

708 Callender, E., 2000. Geochemical effects of rapid sedimentation in aquatic systems: minimal
709 diagenesis and the preservation of historical metal signatures. *J. Paleolimnol.* 23, 243–
710 260. <https://doi.org/10.1023/A:1008114630756>

711 Callender, E., Robbins, J.A., 1993. Transport and accumulation of radionuclides and stable
712 elements in a Missouri River Reservoir. *Water Resour. Res.* 29, 1787–1804.
713 <https://doi.org/10.1029/93WR00387>

714 Carrie, J., Sanei, H., Stern, G., 2012. Standardisation of Rock–Eval pyrolysis for the analysis
715 of recent sediments and soils. *Org. Geochem.* 46, 38–53.
716 <https://doi.org/10.1016/j.orggeochem.2012.01.011>

717 Chawchai, S., Kylander, M.E., Chabangborn, A., Löwemark, L., Wohlfarth, B., 2016. Testing
718 commonly used X-ray fluorescence core scanning-based proxies for organic-rich lake
719 sediments and peat. *Boreas* 45, 180–189. <https://doi.org/10.1111/bor.12145>

720 Chiffoleau, J.-F., Sonke, J.E., Auger, D., Bretaudeau, J., Joguet, T., Larrieu, M., Laffont, L.,
721 Prunier, J., Rozuel, E., Zouiten, C., 2012. Etude de la signature isotopique des métaux
722 dans l'estuaire de la Seine. Une information essentielle pour le traçage et la
723 discrimination des sources et processus.

724 Collins, A.L., Pulley, S., Foster, I.D.L., Gellis, A., Porto, P., Horowitz, A.J., 2017. Sediment
725 source fingerprinting as an aid to catchment management: A review of the current
726 state of knowledge and a methodological decision-tree for end-users. *J. Environ.*
727 *Manage., Sediment source fingerprinting for informing catchment management:*
728 *methodological approaches, problems and uncertainty* 194, 86–108.
729 <https://doi.org/10.1016/j.jenvman.2016.09.075>

730 Copard, Y., Di-Giovanni, C., Martaud, T., Albéric, P., Olivier, J.-E., 2006. Using Rock-Eval 6
731 pyrolysis for tracking fossil organic carbon in modern environments: implications for
732 the roles of erosion and weathering. *Earth Surf. Process. Landf.* 31, 135–153.
733 <https://doi.org/10.1002/esp.1319>

734 Coynel, A., Gorse, L., Curti, C., Schafer, J., Grosbois, C., Morelli, G., Ducassou, E., Blanc,
735 G., Maillet, G.M., Mojtahid, M., 2016. Spatial distribution of trace elements in the
736 surface sediments of a major European estuary (Loire Estuary, France): Source
737 identification and evaluation of anthropogenic contribution. *J. Sea Res., Recent and*
738 *past sedimentary, biogeochemical and benthic ecosystem evolution of the Loire*
739 *Estuary (Western France)* 118, 77–91. <https://doi.org/10.1016/j.seares.2016.08.005>

740 Crutzen, P.J., 2006. The “Anthropocene,” in: Ehlers, E., Krafft, T. (Eds.), *Earth System*
741 *Science in the Anthropocene.* Springer Berlin Heidelberg, Berlin, Heidelberg, pp. 13–
742 18. https://doi.org/10.1007/3-540-26590-2_3

743 Crutzen, P.J., Stoermer, E.F., 2000. The Anthropocene. *Int. Geosphere–Biosphere Programme*
744 *IGBP* 17–18.

745 Debret, M., Chapron, E., Desmet, M., Rolland-Revel, M., Magand, O., Trentesaux, A., Bout-
746 Roumazeille, V., Nomade, J., Arnaud, F., 2010. North western Alps Holocene
747 paleohydrology recorded by flooding activity in Lake Le Bourget, France. *Quat. Sci.*
748 *Rev.* 29, 2185–2200. <https://doi.org/10.1016/j.quascirev.2010.05.016>

749 Debret, M., Desmet, M., Balsam, W., Copard, Y., Francus, P., Laj, C., 2006.
750 Spectrophotometer analysis of Holocene sediments from an anoxic fjord: Saanich
751 Inlet, British Columbia, Canada. *Mar. Geol.* 229, 15–28.
752 <https://doi.org/10.1016/j.margeo.2006.01.005>

753 Debret, M., Sebag, D., Desmet, M., Balsam, W., Copard, Y., Mourier, B., Susperrigui, A.-S.,
754 Arnaud, F., Bentaleb, I., Chapron, E., Lallier-Vergès, E., Winiarski, T., 2011.
755 Spectrocolorimetric interpretation of sedimentary dynamics: The new “Q7/4 diagram.”
756 *Earth-Sci. Rev.* 109, 1–19. <https://doi.org/10.1016/j.earscirev.2011.07.002>

757 Devault, D.A., Gérino, M., Laplanche, C., Julien, F., Winterton, P., Merlina, G., Delmas, F.,
758 Lim, P., Miguel Sánchez-Pérez, J., Pinelli, E., 2009. Herbicide accumulation and
759 evolution in reservoir sediments. *Sci. Total Environ.* 407, 2659–2665.
760 <https://doi.org/10.1016/j.scitotenv.2008.12.064>

761 Dhivert, E., Grosbois, C., Coynel, A., Lefèvre, I., Desmet, M., 2015. Influences of major
762 flood sediment inputs on sedimentary and geochemical signals archived in a reservoir
763 core (Upper Loire Basin, France). *CATENA* 126, 75–85.
764 <https://doi.org/10.1016/j.catena.2014.10.030>

765 Dickinson, W.W., Dunbar, G.B., McLeod, H., 1996. Heavy metal history from cores in
766 Wellington Harbour, New Zealand. *Environ. Geol.* 27, 59–69.
767 <https://doi.org/10.1007/BF00770603>

768 Disnar, J.R., Guillet, B., Keravis, D., Di-Giovanni, C., Sebag, D., 2003. Soil organic matter
769 (SOM) characterization by Rock-Eval pyrolysis: scope and limitations. *Org.*
770 *Geochem.* 34, 327–343. [https://doi.org/10.1016/S0146-6380\(02\)00239-5](https://doi.org/10.1016/S0146-6380(02)00239-5)

771 Duan, D., Ran, Y., Cheng, H., Chen, J., Wan, G., 2014. Contamination trends of trace metals
772 and coupling with algal productivity in sediment cores in Pearl River Delta, South
773 China. *Chemosphere* 103, 35–43. <https://doi.org/10.1016/j.chemosphere.2013.11.011>

774 Evans, J.E., 2015. Contaminated Sediment and Dam Removals: Problem or Opportunity? *Eos*
775 96, 10. <https://doi.org/doi:10.1029/2015EO036385>

776 Ferrand, E., Eyrolle, F., Radakovitch, O., Provansal, M., Dufour, S., Vella, C., Raccasi, G.,
777 Gurriaran, R., 2012. Historical levels of heavy metals and artificial radionuclides
778 reconstructed from overbank sediment records in lower Rhône River (South-East
779 France). *Geochim. Cosmochim. Acta, Environmental Records of Anthropogenic*
780 *Impacts* 82, 163–182. <https://doi.org/10.1016/j.gca.2011.11.023>

781 Folke, C., Carpenter, S., Elmqvist, T., Gunderson, L., Holling, C.S., Walker, B., 2002.
782 Resilience and Sustainable Development: Building Adaptive Capacity in a World of
783 Transformations. *AMBIO J. Hum. Environ.* 31, 437–440.
784 <https://doi.org/10.1579/0044-7447-31.5.437>

785 Gil-García, C., Rigol, A., Vidal, M., 2009. New best estimates for radionuclide solid–liquid
786 distribution coefficients in soils, Part 1: radiostrontium and radiocaesium. *J. Environ.*
787 *Radioact.* 100, 690–696. <https://doi.org/10.1016/j.jenvrad.2008.10.003>

788 Grosbois, C., Meybeck, M., Horowitz, A., Ficht, A., 2006. The spatial and temporal trends of
789 Cd, Cu, Hg, Pb and Zn in Seine River floodplain deposits (1994–2000). *Sci. Total*
790 *Environ.* 356, 22–37. <https://doi.org/10.1016/j.scitotenv.2005.01.049>

791 Grygar, T.M., Elznicová, J., Kiss, T., Smith, H., 2016. Using sedimentary archives to
792 reconstruct pollution history and sediment provenance: the Ohře River, Czech
793 Republic. *Catena* 144, 109–129.

794 Gu, Z., Shi, C., Yang, H., Yao, H., 2019. Analysis of dynamic sedimentary environments in
795 alluvial fans of some tributaries of the upper Yellow River of China based on ground
796 penetrating radar (GPR) and sediment cores. *Quat. Int., BRIDGING EUROPE AND*
797 *ASIA: QUATERNARY STRATIGRAPHY AND PALAEOLOGICAL HUMAN*
798 *OCCUPATION* 509, 30–40. <https://doi.org/10.1016/j.quaint.2018.05.001>

799 Guédron, S., Amouroux, D., Sabatier, P., Desplanque, C., Develle, A.-L., Barre, J., Feng, C.,
800 Guiter, F., Arnaud, F., Reyss, J.L., Charlet, L., 2016. A hundred year record of
801 industrial and urban development in French Alps combining Hg accumulation rates
802 and isotope composition in sediment archives from Lake Luitel. *Chem. Geol.* 431, 10–
803 19. <https://doi.org/10.1016/j.chemgeo.2016.03.016>

804 Guermond, Y., 1981. Louviers - Le Vaudreuil : l'impact spatial d'un pôle d'emploi comme
805 moyen d'évaluation du changement social. *Noroi* 112, 577–598.
806 <https://doi.org/10.3406/noroi.1981.3996>

807 Hanesch, M., Scholger, R., 2002. Mapping of heavy metal loadings in soils by means of
808 magnetic susceptibility measurements. *Environ. Geol.* 42, 857–870.
809 <https://doi.org/10.1007/s00254-002-0604-1>

810 Hatfield, R.G., Maher, B.A., 2009. Fingerprinting upland sediment sources: particle size-
811 specific magnetic linkages between soils, lake sediments and suspended sediments.
812 *Earth Surf. Process. Landf.* 34, 1359–1373. <https://doi.org/10.1002/esp.1824>

813 Hatfield, R.G., Maher, B.A., 2008. Suspended sediment characterization and tracing using a
814 magnetic fingerprinting technique: Bassenthwaite Lake, Cumbria, UK. *The Holocene*
815 18, 105–115. <https://doi.org/10.1177/0959683607085600>

816 Hatfield, R.G., Stoner, J.S., 2013. Magnetic Proxies and Susceptibility. *Elias SA Ed Encycl.*
817 *Quat. Sci.* 2, 884–898.

818 He, Q., Walling, D.E., 1996. Interpreting particle size effects in the adsorption of ¹³⁷Cs and
819 unsupported ²¹⁰Pb by mineral soils and sediments. *J. Environ. Radioact.* 30, 117–137.
820 [https://doi.org/10.1016/0265-931X\(96\)89275-7](https://doi.org/10.1016/0265-931X(96)89275-7)

821 Hennekam, R., Sweere, T., Tjallingii, R., de Lange, G.J., Reichart, G.-J., 2019. Trace metal
822 analysis of sediment cores using a novel X-ray fluorescence core scanning method.
823 *Quat. Int., Advances in Data Quantification and Application of high resolution XRF*
824 *Core Scanners* 514, 55–67. <https://doi.org/10.1016/j.quaint.2018.10.018>

825 Holling, C.S., 1973. Resilience and Stability of Ecological Systems. *Annu. Rev. Ecol. Syst.* 4,
826 1–23. <https://doi.org/10.1146/annurev.es.04.110173.000245>

827 Horowitz, A.J., Elrick, K.A., 1987. The relation of stream sediment surface area, grain size
828 and composition to trace element chemistry. *Appl. Geochem.* 2, 437–451.
829 [https://doi.org/10.1016/0883-2927\(87\)90027-8](https://doi.org/10.1016/0883-2927(87)90027-8)

830 Horowitz, A.J., Elrick, K.A., Callender, E., 1988. The effect of mining on the sediment - trace
831 element geochemistry of cores from the Cheyenne River arm of Lake Oahe, South
832 Dakota, U.S.A. *Chem. Geol.* 67, 17–33. [https://doi.org/10.1016/0009-2541\(88\)90003-](https://doi.org/10.1016/0009-2541(88)90003-4)
833 4

834 Horowitz, A.J., Meybeck, M., Idlalkih, Z., Biger, E., 1999. Variations in trace element
835 geochemistry in the Seine River Basin based on floodplain deposits and bed
836 sediments. *Hydrol. Process.* 13, 1329–1340. [https://doi.org/10.1002/\(SICI\)1099-](https://doi.org/10.1002/(SICI)1099-1085(19990630)13:9<1329::AID-HYP811>3.0.CO;2-H)
837 1085(19990630)13:9<1329::AID-HYP811>3.0.CO;2-H

838 Huguenberger, P., Meier, E., Pugin, A., 1994. Ground-probing radar as a tool for
839 heterogeneity estimation in gravel deposits: advances in data-processing and facies
840 analysis. *J. Appl. Geophys., Geophysics and Environment* 31, 171–184.
841 [https://doi.org/10.1016/0926-9851\(94\)90056-6](https://doi.org/10.1016/0926-9851(94)90056-6)

842 Huguenberger, P., Regli, C., 2006. A Sedimentological Model to Characterize Braided River
843 Deposits for Hydrogeological Applications, in: Sambrook Smith, G.H., Best, J.L.,
844 Bristow, C.S., Petts, G.E. (Eds.), *Braided Rivers*. Blackwell Publishing Ltd., Oxford,
845 UK, pp. 51–74. <https://doi.org/10.1002/9781444304374.ch3>

846 IREP - Registre des Emissions Polluantes [WWW Document], n.d. URL
847 [http://www.georisques.gouv.fr/cartes-](http://www.georisques.gouv.fr/cartes-interactive/#/show/http%3A%2F%2Fmapsref.brgm.fr%2Fwxs%2Fgeorisques%2Frisques%3Fid_query%3D9613/ETABLISSEMENTS_POLLUEURS_RECHERCHE/)
848 [interactive/#/show/http%3A%2F%2Fmapsref.brgm.fr%2Fwxs%2Fgeorisques%2Frisques%3Fid_query%3D9613/ETABLISSEMENTS_POLLUEURS_RECHERCHE/](http://www.georisques.gouv.fr/cartes-interactive/#/show/http%3A%2F%2Fmapsref.brgm.fr%2Fwxs%2Fgeorisques%2Frisques%3Fid_query%3D9613/ETABLISSEMENTS_POLLUEURS_RECHERCHE/)-
849 [ETABLISSEMENTS_POLLUEURS_RECHERCHE/](http://www.georisques.gouv.fr/cartes-interactive/#/show/http%3A%2F%2Fmapsref.brgm.fr%2Fwxs%2Fgeorisques%2Frisques%3Fid_query%3D9613/ETABLISSEMENTS_POLLUEURS_RECHERCHE/)

850 357823.2365,6037008.6939,1313632.3628,7230727.3772/EPSG:2154 (accessed
851 4.25.19).

852 James, L.A., 2018. Ten conceptual models of large-scale legacy sedimentation – A review.
853 *Geomorphology* 317, 199–217. <https://doi.org/10.1016/j.geomorph.2018.05.021>

854 James, L.A., 2013. Legacy sediment: Definitions and processes of episodically produced
855 anthropogenic sediment. *Anthropocene, Geomorphology of the Anthropocene:
856 Understanding The Surficial Legacy of Past and Present Human Activities* 2, 16–26.
857 <https://doi.org/10.1016/j.ancene.2013.04.001>

858 Kaci, A., Petit, F., Fournier, M., Cécillon, S., Boust, D., Lesueur, P., Berthe, T., 2016.
859 Diversity of active microbial communities subjected to long-term exposure to
860 chemical contaminants along a 40-year-old sediment core. *Environ. Sci. Pollut. Res.*
861 23, 4095–4110. <https://doi.org/10.1007/s11356-015-4506-7>

862 Kaci, A., Petit, F., Lesueur, P., Boust, D., Vrel, A., Berthe, T., 2014. Distinct diversity of the
863 *czcA* gene in two sedimentary horizons from a contaminated estuarine core. *Environ.*
864 *Sci. Pollut. Res.* 21, 10787–10802. <https://doi.org/10.1007/s11356-014-3029-y>

865 Knab, M., Hoffmann, V., Petrovský, E., Kapička, A., Jordanova, N., Appel, E., 2006.
866 Surveying the anthropogenic impact of the Moldau river sediments and nearby soils
867 using magnetic susceptibility. *Environ. Geol.* 49, 527–535.
868 <https://doi.org/10.1007/s00254-005-0080-5>

869 Koiter, A.J., Owens, P.N., Petticrew, E.L., Lobb, D.A., 2013. The behavioural characteristics
870 of sediment properties and their implications for sediment fingerprinting as an
871 approach for identifying sediment sources in river basins. *Earth-Sci. Rev.* 125, 24–42.
872 <https://doi.org/10.1016/j.earscirev.2013.05.009>

873 Kostic, B., Becht, A., Aigner, T., 2005. 3-D sedimentary architecture of a Quaternary gravel
874 delta (SW-Germany): Implications for hydrostratigraphy. *Sediment. Geol.* 181, 147–
875 171. <https://doi.org/10.1016/j.sedgeo.2005.07.004>

876 Krishnaswamy, S., Lal, D., Martin, J.M., Meybeck, M., 1971. Geochronology of lake
877 sediments. *Earth Planet. Sci. Lett.* 11, 407–414. [https://doi.org/10.1016/0012-821X\(71\)90202-0](https://doi.org/10.1016/0012-821X(71)90202-0)

878

879 Kurashige, Y., Fusejima, Y., 1997. Source identification of suspended sediment from grain-
880 size distributions: I. Application of nonparametric statistical tests. *CATENA* 31, 39–
881 52. [https://doi.org/10.1016/S0341-8162\(97\)00033-7](https://doi.org/10.1016/S0341-8162(97)00033-7)

882 Kylander, M.E., Ampel, L., Wohlfarth, B., Veres, D., 2011. High-resolution X-ray
883 fluorescence core scanning analysis of Les Echets (France) sedimentary sequence:
884 new insights from chemical proxies. *J. Quat. Sci.* 26, 109–117.
885 <https://doi.org/10.1002/jqs.1438>

886 Laignel, B., Quesnel, F., Lecoustumer, M.-N., Meyer, R., 1998. Variabilité du cortège
887 argileux des formations résiduelles à silex de l’Ouest du bassin de Paris. *Comptes
888 Rendus Académie Sci. - Ser. IIA - Earth Planet. Sci.* 326, 467–472.
889 [https://doi.org/10.1016/S1251-8050\(98\)80072-4](https://doi.org/10.1016/S1251-8050(98)80072-4)

890 Le Cloarec, M.-F., Bonte, P.H., Lestel, L., Lefèvre, I., Ayrault, S., 2011. Sedimentary record
891 of metal contamination in the Seine River during the last century. *Phys. Chem. Earth
892 Parts ABC, Man and River Systems: From pressures to physical, chemical and
893 ecological status* 36, 515–529. <https://doi.org/10.1016/j.pce.2009.02.003>

894 Lepland, Aivo, Andersen, T.J., Lepland, Aave, Arp, H.P.H., Alve, E., Breedveld, G.D.,
895 Rindby, A., 2010. Sedimentation and chronology of heavy metal pollution in Oslo
896 harbor, Norway. *Mar. Pollut. Bull.* 60, 1512–1522.
897 <https://doi.org/10.1016/j.marpolbul.2010.04.017>

898 Lestel, L., Eschbach, D., Steinmann, R., Gastaldi, N., 2019. *ArchiSEINE : une approche
899 géohistorique du bassin de la Seine* (No. 18).

- 900 Lewis, S.L., Maslin, M.A., 2015. Defining the Anthropocene. *Nature* 519, 171–180.
901 <https://doi.org/10.1038/nature14258>
- 902 Lin, Y.-T., Schuettelpelz, C.C., Wu, C.H., Fratta, D., 2009. A combined acoustic and
903 electromagnetic wave-based techniques for bathymetry and subbottom profiling in
904 shallow waters. *J. Appl. Geophys.* 68, 203–218.
905 <https://doi.org/10.1016/j.jappgeo.2008.11.010>
- 906 Livens, F.R., Baxter, M.S., 1988. Particle size and radionuclide levels in some west Cumbrian
907 soils. *Sci. Total Environ., Environmental Radiochemical Analysis* 70, 1–17.
908 [https://doi.org/10.1016/0048-9697\(88\)90248-3](https://doi.org/10.1016/0048-9697(88)90248-3)
- 909 Lorgeoux, C., Moilleron, R., Gasperi, J., Ayrault, S., Bonté, P., Lefèvre, I., Tassin, B., 2016.
910 Temporal trends of persistent organic pollutants in dated sediment cores: Chemical
911 fingerprinting of the anthropogenic impacts in the Seine River basin, Paris. *Sci. Total*
912 *Environ.* 541, 1355–1363. <https://doi.org/10.1016/j.scitotenv.2015.09.147>
- 913 Mabit, L., Benmansour, M., Abril, J.M., Walling, D.E., Meusburger, K., Iurian, A.R.,
914 Bernard, C., Tarján, S., Owens, P.N., Blake, W.H., Alewell, C., 2014. Fallout ²¹⁰Pb
915 as a soil and sediment tracer in catchment sediment budget investigations: A review.
916 *Earth-Sci. Rev.* 138, 335–351. <https://doi.org/10.1016/j.earscirev.2014.06.007>
- 917 Magiera, T., Strzyszcz, Z., Kapicka, A., Petrovsky, E., 2006. Discrimination of lithogenic and
918 anthropogenic influences on topsoil magnetic susceptibility in Central Europe.
919 *Geoderma* 130, 299–311. <https://doi.org/10.1016/j.geoderma.2005.02.002>
- 920 Masson, M., Blanc, G., Schäfer, J., 2006. Geochemical signals and source contributions to
921 heavy metal (Cd, Zn, Pb, Cu) fluxes into the Gironde Estuary via its major tributaries.
922 *Sci. Total Environ.* 370, 133–146. <https://doi.org/10.1016/j.scitotenv.2006.06.011>
- 923 Masson, M., Blanc, G., Schäfer, J., Parlanti, E., Le Coustumer, P., 2011. Copper addition by
924 organic matter degradation in the freshwater reaches of a turbid estuary. *Sci. Total*
925 *Environ.* 409, 1539–1549. <https://doi.org/10.1016/j.scitotenv.2011.01.022>
- 926 Mellett, J.S., 1995. Profiling of ponds and bogs using ground-penetrating radar. *J.*
927 *Paleolimnol.* 14, 233–240. <https://doi.org/10.1007/BF00682425>
- 928 Meybeck, M., Lestel, L., Bonté, P., Moilleron, R., Colin, J.L., Rousselot, O., Hervé, D., de
929 Pontevès, C., Grosbois, C., Thévenot, D.R., 2007. Historical perspective of heavy
930 metals contamination (Cd, Cr, Cu, Hg, Pb, Zn) in the Seine River basin (France)
931 following a DPSIR approach (1950–2005). *Sci. Total Environ., Human activity and*
932 *material fluxes in a regional river basin: the Seine River watershed* 375, 204–231.
933 <https://doi.org/10.1016/j.scitotenv.2006.12.017>
- 934 Monna, F., Lancelot, J., Bernat, M., Mercadier, H., 1998. Sedimentation rate in the Thau
935 basin (France) according to geochronological, geochemical and stratigraphical data.
936 *Oceanogr. Lit. Rev.* 2, 279–280.
- 937 Müller, J., Ruppert, H., Muramatsu, Y., Schneider, J., 2000. Reservoir sediments – a witness
938 of mining and industrial development (Malter Reservoir, eastern Erzgebirge,
939 Germany). *Environ. Geol.* 39, 1341–1351. <https://doi.org/10.1007/s002540000117>
- 940 Neal, A., 2004. Ground-penetrating radar and its use in sedimentology: principles, problems
941 and progress. *Earth-Sci. Rev.* 66, 261–330.
942 <https://doi.org/10.1016/j.earscirev.2004.01.004>
- 943 Nguyen, H.L., Braun, M., Szaloki, I., Baeyens, W., Van Grieken, R., Leermakers, M., 2009.
944 Tracing the Metal Pollution History of the Tisza River Through the Analysis of a
945 Sediment Depth Profile. *Water. Air. Soil Pollut.* 200, 119–132.
946 <https://doi.org/10.1007/s11270-008-9898-2>
- 947 Nilsson, C., Reidy, C.A., Dynesius, M., Revenga, C., 2005. Fragmentation and Flow
948 Regulation of the World's Large River Systems. *Science* 308, 405–408.
949 <https://doi.org/10.1126/science.1107887>

- 950 O’Driscoll, M., Johnson, P., Mallinson, D., 2010. Geological controls and effects of
951 floodplain asymmetry on river–groundwater interactions in the southeastern Coastal
952 Plain, USA. *Hydrogeol. J.* 18, 1265–1279. <https://doi.org/10.1007/s10040-010-0595-z>
- 953 Petit, J.C.J., Schäfer, J., Coynel, A., Blanc, G., Deycard, V.N., Derriennic, H., Lancelleur, L.,
954 Dutruch, L., Bossy, C., Mattielli, N., 2013. Anthropogenic sources and
955 biogeochemical reactivity of particulate and dissolved Cu isotopes in the turbidity
956 gradient of the Garonne River (France). *Chem. Geol.* 359, 125–135.
957 <https://doi.org/10.1016/j.chemgeo.2013.09.019>
- 958 Pittam, N.J., Foster, I.D.L., Mighall, T.M., 2009. An integrated lake-catchment approach for
959 determining sediment source changes at Aqualate Mere, Central England. *J.*
960 *Paleolimnol.* 42, 215–232. <https://doi.org/10.1007/s10933-008-9272-9>
- 961 Pulley, S., Van der Waal, B., Rowntree, K., Collins, A.L., 2018. Colour as reliable tracer to
962 identify the sources of historically deposited flood bench sediment in the Transkei,
963 South Africa: A comparison with mineral magnetic tracers before and after hydrogen
964 peroxide pre-treatment. *CATENA* 160, 242–251.
965 <https://doi.org/10.1016/j.catena.2017.09.018>
- 966 Quesnel, F., 1997. Digital mapping in regolith geology. *Cartographie numérique en géologie*
967 *de surface. Application aux altérites à silex de l’Ouest du bassin de Paris (Theses).*
968 Université de Rouen.
- 969 Richter, T.O., Gaast, S. van der, Koster, B., Vaars, A., Gieles, R., Stigter, H.C. de, Haas,
970 H.D., Weering, T.C.E. van, 2006. The Avaatech XRF Core Scanner: technical
971 description and applications to NE Atlantic sediments. *Geol. Soc. Lond. Spec. Publ.*
972 267, 39–50. <https://doi.org/10.1144/GSL.SP.2006.267.01.03>
- 973 Robbins, J.A., Edgington, D.N., 1975. Determination of recent sedimentation rates in Lake
974 Michigan using Pb-210 and Cs-137. *Geochim. Cosmochim. Acta* 39, 285–304.
975 [https://doi.org/10.1016/0016-7037\(75\)90198-2](https://doi.org/10.1016/0016-7037(75)90198-2)
- 976 Sabatier, P., Poulenard, J., Fanget, B., Reyss, J.-L., Develle, A.-L., Wilhelm, B., Ployon, E.,
977 Pignol, C., Naffrechoux, E., Dorioz, J.-M., Montuelle, B., Arnaud, F., 2014. Long-
978 term relationships among pesticide applications, mobility, and soil erosion in a
979 vineyard watershed. *Proc. Natl. Acad. Sci. U. S. A.* 111, 15647–15652.
980 <https://doi.org/10.1073/pnas.1411512111>
- 981 Sebag, D., Debret, M., M’voubou, M., Obame, R.M., Ngomanda, A., Oslisly, R., Bentaleb, I.,
982 Disnar, J.-R., Giresse, P., 2013. Coupled Rock-Eval pyrolysis and spectrophotometry
983 for lacustrine sedimentary dynamics: Application for West Central African rainforests
984 (Kamalété and Nguène lakes, Gabon). *The Holocene* 23, 1173–1183.
985 <https://doi.org/10.1177/0959683613483622>
- 986 Sebok, E., Karan, S., Engesgaard, P., 2018. Using hydrogeophysical methods to assess the
987 feasibility of lake bank filtration. *J. Hydrol.* 562, 423–434.
988 <https://doi.org/10.1016/j.jhydrol.2018.04.049>
- 989 Shuman, J.R., 1995. Environmental considerations for assessing dam removal alternatives for
990 river restoration. *Regul. Rivers Res. Manag.* 11, 249–261.
991 <https://doi.org/10.1002/rrr.3450110302>
- 992 Singh, N., Li, J., Zeng, X., 2016. Solutions and challenges in recycling waste cathode-ray
993 tubes. *J. Clean. Prod.* 133, 188–200. <https://doi.org/10.1016/j.jclepro.2016.04.132>
- 994 Słowik, M., 2015. Is history of rivers important in restoration projects? The example of
995 human impact on a lowland river valley (the Odra River, Poland). *Geomorphology,*
996 *Emerging geomorphic approaches to guide river management practices* 251, 50–63.
997 <https://doi.org/10.1016/j.geomorph.2015.05.031>
- 998 Stanley, E.H., Doyle, M.W., 2003. Trading off: the ecological effects of dam removal. *Front.*
999 *Ecol. Environ.* 1, 15–22. [https://doi.org/10.1890/1540-9295\(2003\)001\[0015:TOTEEO\]2.0.CO;2](https://doi.org/10.1890/1540-9295(2003)001[0015:TOTEEO]2.0.CO;2)
- 1000

- 1001 Steffen, W., Grinevald, J., Crutzen, P., McNeill, J., 2011. The Anthropocene: conceptual and
1002 historical perspectives. *Philos. Trans. R. Soc. Math. Phys. Eng. Sci.* 369, 842–867.
1003 <https://doi.org/10.1098/rsta.2010.0327>
- 1004 Tamtam, F., Le Bot, B., Dinh, T., Mompelat, S., Eurin, J., Chevreuil, M., Bonté, P., Mouchel,
1005 J.-M., Ayrault, S., 2011. A 50-year record of quinolone and sulphonamide
1006 antimicrobial agents in Seine River sediments. *J. Soils Sediments* 11, 852–859.
1007 <https://doi.org/10.1007/s11368-011-0364-1>
- 1008 Thibert, S., 1994. Exportations naturelles et anthropiques des ions majeurs et des éléments
1009 nutritifs dans le bassin de la Seine : approches méthodologiques. Université Pierre et
1010 Marie Curie - Paris VI.
- 1011 Tissot, B.P., Welte, D.H., 1984. *Petroleum Formation and Occurrence*, 2nd edition. ed.
1012 Springer, Heidelberg.
- 1013 Toonen, W.H.J., Winkels, T.G., Cohen, K.M., Prins, M.A., Middelkoop, H., 2015. Lower
1014 Rhine historical flood magnitudes of the last 450 years reproduced from grain-size
1015 measurements of flood deposits using End Member Modelling. *CATENA, Past
1016 Hydrological Extreme Events in a Changing Climate* 130, 69–81.
1017 <https://doi.org/10.1016/j.catena.2014.12.004>
- 1018 Tseng, C.M., Amouroux, D., Abril, G., Tessier, E., Etcheber, H., Donard, O.F.X., 2001.
1019 Speciation of Mercury in a Fluid Mud Profile of a Highly Turbid Macrotidal Estuary
1020 (Gironde, France). *Environ. Sci. Technol.* 35, 2627–2633.
1021 <https://doi.org/10.1021/es001750b>
- 1022 Tsydenova, O., Bengtsson, M., 2011. Chemical hazards associated with treatment of waste
1023 electrical and electronic equipment. *Waste Manag.* 31, 45–58.
1024 <https://doi.org/10.1016/j.wasman.2010.08.014>
- 1025 Van Metre, P.C., Callender, E., Fuller, C.C., 1997. Historical Trends in Organochlorine
1026 Compounds in River Basins Identified Using Sediment Cores from Reservoirs.
1027 *Environ. Sci. Technol.* 31, 2339–2344. <https://doi.org/10.1021/es960943p>
- 1028 Van Metre, P.C., Mesnage, V., Laignel, B., Motelay, A., Deloffre, J., 2008. Origins of
1029 Sediment-Associated Contaminants to the Marais Vernier, the Seine Estuary, France.
1030 *Water. Air. Soil Pollut.* 191, 331–344. <https://doi.org/10.1007/s11270-008-9628-9>
- 1031 Vrel, A., 2012. Reconstitution de l’historique des apports en radionucléides et contaminants
1032 métalliques à l’estuaire fluvial de la Seine par l’analyse de leur enregistrement
1033 sédimentaire.
- 1034 Vrel, A., Boust, D., Lesueur, P., Deloffre, J., Dubrulle-Brunaud, C., Solier, L., Rozet, M.,
1035 Thouroude, C., Cossonnet, C., Thomas, S., 2013. Dating of sediment record at two
1036 contrasting sites of the Seine River using radioactivity data and hydrological time
1037 series. *J. Environ. Radioact.* 126, 20–31. <https://doi.org/10.1016/j.jenvrad.2013.06.005>
- 1038 Walling, D.E., Owens, P.N., Carter, J., Leeks, G.J.L., Lewis, S., Meharg, A.A., Wright, J.,
1039 2003. Storage of sediment-associated nutrients and contaminants in river channel and
1040 floodplain systems. *Appl. Geochem.* 18, 195–220. [https://doi.org/10.1016/S0883-
1041 2927\(02\)00121-X](https://doi.org/10.1016/S0883-2927(02)00121-X)
- 1042 Walling, D.E., Woodward, J.C., 1992. Use of radiometric fingerprints to derive information
1043 on suspended sediment sources. *Eros. Sediment Transp. Monit. Programme River
1044 Basins* 153–64.
- 1045 Wang, K., Cornett, R.J., 1993. Distribution coefficients of ^{210}Pb and ^{210}Po in laboratory and
1046 natural aquatic systems. *J. Paleolimnol.* 9, 179–188.
1047 <https://doi.org/10.1007/BF00677519>
- 1048 Weltje, G.J., 2012. Quantitative models of sediment generation and provenance: State of the
1049 art and future developments. *Sediment. Geol., Actualistic Models of Sediment
1050 Generation* 280, 4–20. <https://doi.org/10.1016/j.sedgeo.2012.03.010>

1051 Winkels, H.J., Kroonenberg, S.B., Lychagin, M.Y., Marin, G., Rusakov, G.V., Kasimov,
1052 N.S., 1998. Geochronology of priority pollutants in sedimentation zones of the Volga
1053 and Danube delta in comparison with the Rhine delta. *Appl. Geochem.* 13, 581–591.
1054 [https://doi.org/10.1016/S0883-2927\(98\)00002-X](https://doi.org/10.1016/S0883-2927(98)00002-X)
1055 Yang, Z., Wang, H., Saito, Y., Milliman, J.D., Xu, K., Qiao, S., Shi, G., 2006. Dam impacts
1056 on the Changjiang (Yangtze) River sediment discharge to the sea: The past 55 years
1057 and after the Three Gorges Dam. *Water Resour. Res.* 42.
1058 <https://doi.org/10.1029/2005WR003970>
1059

Figure 1. A. Historic sediment core sites in the lower reaches of the Seine River watershed and sediment core sites in the Eure River (present study). The length, time period represented and chemicals elements studied for each core sites are also mentioned; B. The Eure River watershed (present study). The Yonne and Oise rivers sub-watersheds studied in Ayrault et al., 2010b and Le Cloarec et al., 2011 are also represented.

Figure 2. Morphological modifications of Martot Pond and Les Damps Pond study sites established from several unpublished documents (e.g. maps from “Pont et Chaussées” and meeting minutes) stored at “Voie Navigable de France” (VNF). The cities of Martot, Pont-de-l’Arche et Les Damps have been indicated on the maps to facilitate comparison with the actual study area.

Figure 3. A. Study Area; B. Sediment core and GPR profiles locations in Les Damps Pond; C. Sediment core and GPR profiles locations in Martot Pond.

Figure 4. A1. Colour log; and B. Grain size distribution and D_{50} ; A2. Colour log; C. TOC, HI, and OI; D. Magnetic susceptibility (MS) and reflectance (L^*); E. First derivative values; F. Pb/Ti, Zn/Ti, Cu/Ti, and Ni/Ti ratios along the DAM15-02 and DAM17-02 cores collected in Les Damps Pond.

Figure 5. A. Colour log; B. Grain size distribution and D_{50} ; C. TOC, HI, and OI; D. Magnetic susceptibility (MS) and reflectance (L^*); E. First derivative values; F. Pb/Ti, Zn/Ti, Cu/Ti and Ni/Ti ratios along MAR15-01 core collected in Martot Pond.

Figure 6. Pb/Ti, Zn/Ti, and Cu/Ti ratios along the upper part of the MAR16-02 core. Pb (dark circle), Zn (dark square) and Cu (dark triangle) concentrations are also presented.

Figure 7. A. $^{210}\text{Pb}_{\text{ex}}$; B. ^{137}Cs and ^{241}Am ; C. Age model for the MAR15-01 core.

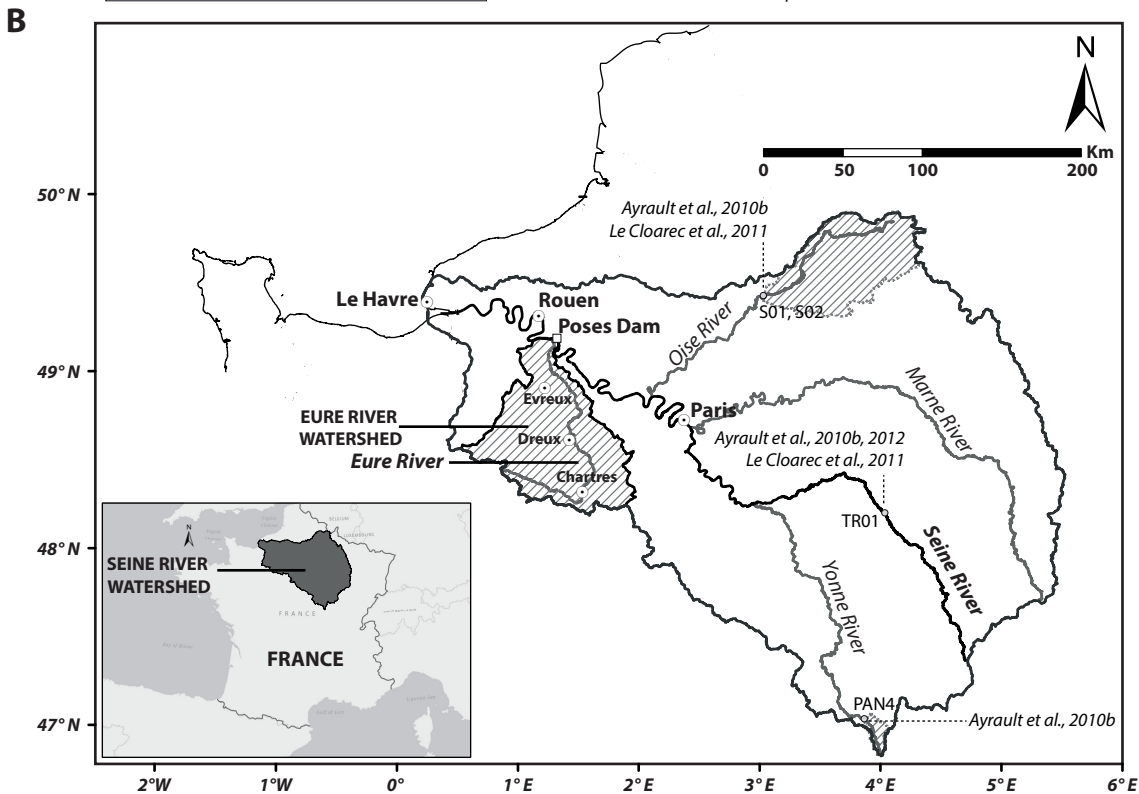
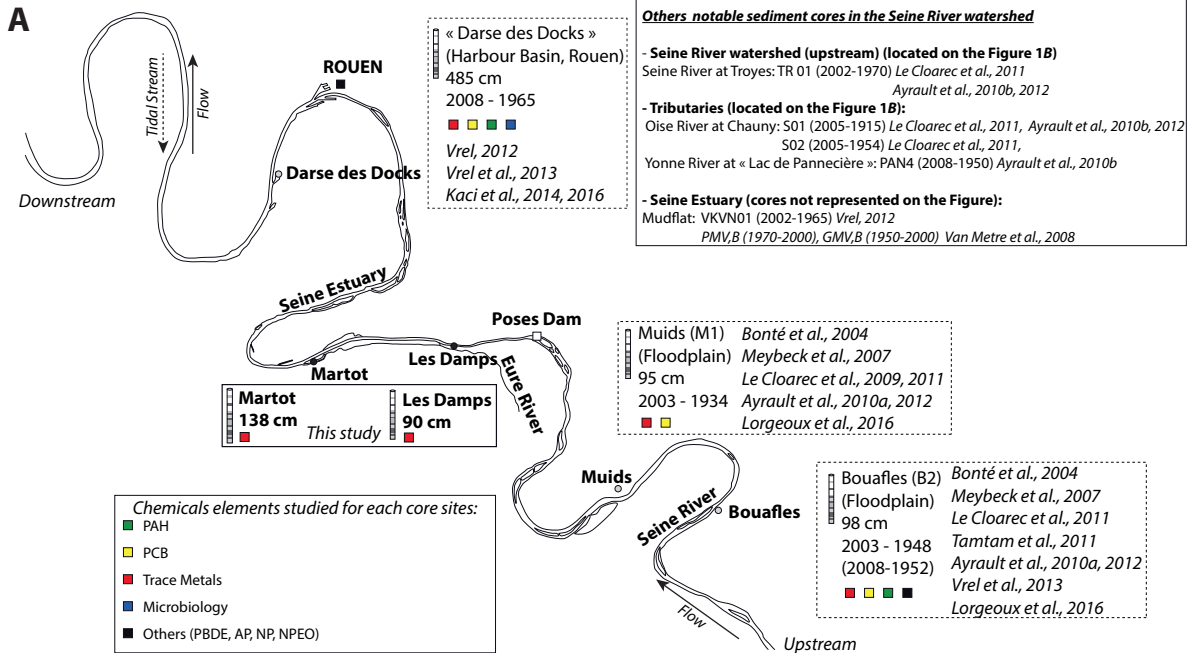
Figure 8. Radargram performed with a 400 mHz antenna, migration rate used: 0.075 m ns^{-1} . Due to the lengths and depths reached and to obtain adequate readability, the x-scales of the 3 profiles are different. For reasons of navigability, all the core sampling points previously presented could not be documented by GPR, in particular the MAR15-01 and DAM15-02 cores. A. GPR-MAR_08 radargram, processed and interpreted from Martot Pond. To obtain a 2D information, the MAR15-02, MAR15-03, MAR15-04, and MAR15-06 cores with a simple description distinguishing only the U1 and U2 facies, have been positioned; B. GPR_DAM_03 radargram processed and interpreted from Les Damps Pond. The DAM15-03 and DAM18-02 cores have been positioned; C. GRP_DAM_05 radargram, processed and interpreted from Les Damps Pond. The DAM17-02 core has been positioned.

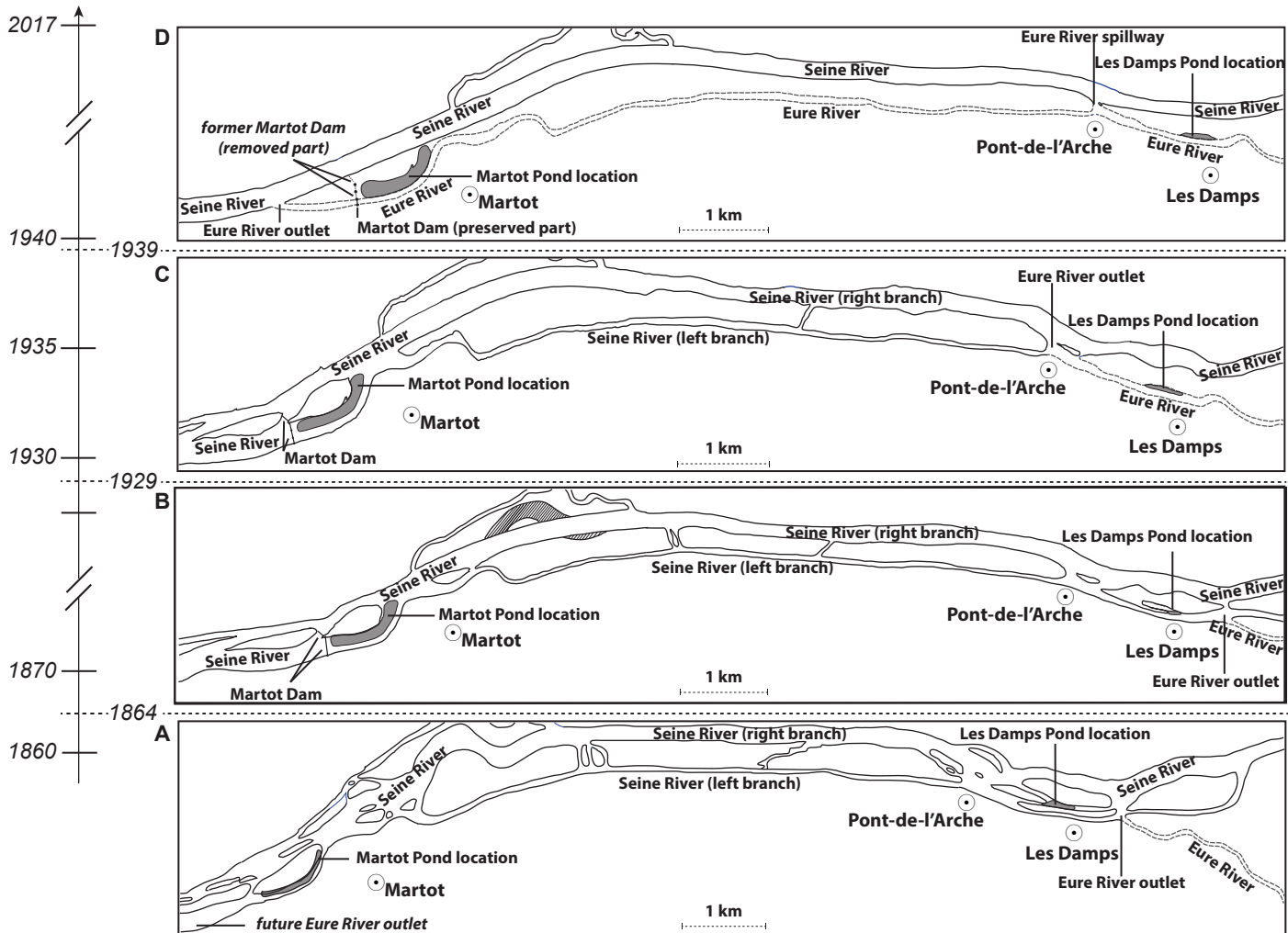
Figure 9. A. Pseudo Van-Krevelen diagram; B. Q7/4 vs L* ratio for the MAR15-01 core (U1 and U2 facies) and the DAM17-02 core.

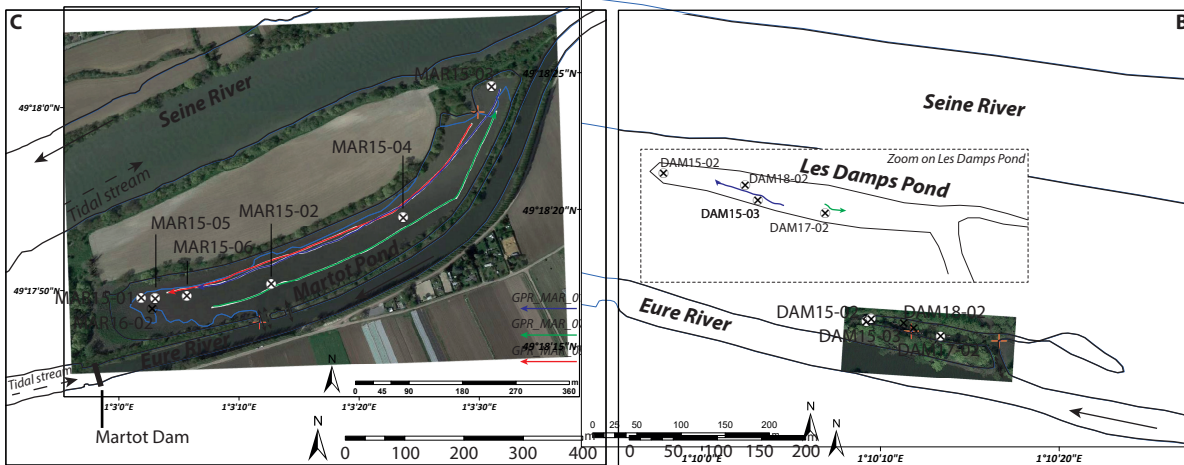
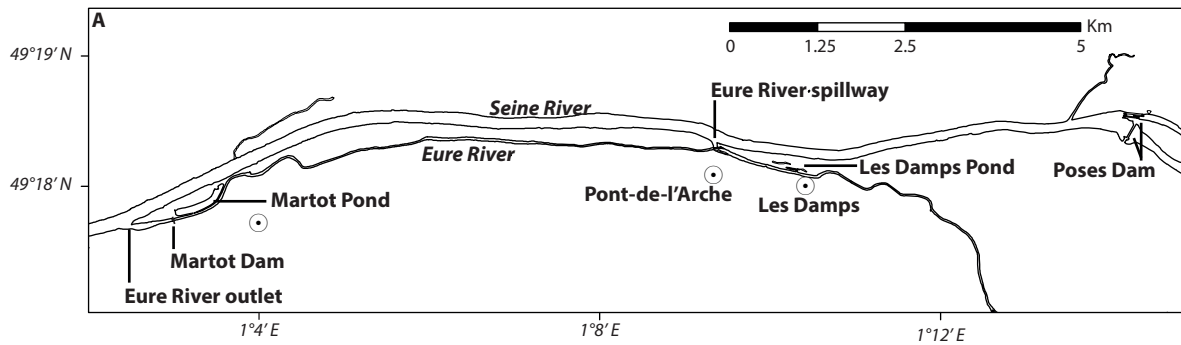
Figure 10. Evolution of Pb/Ti, Zn/Ti, Cu/Ti, and Ni/Ti ratios along the Eure Unit (MAR15-01 core).

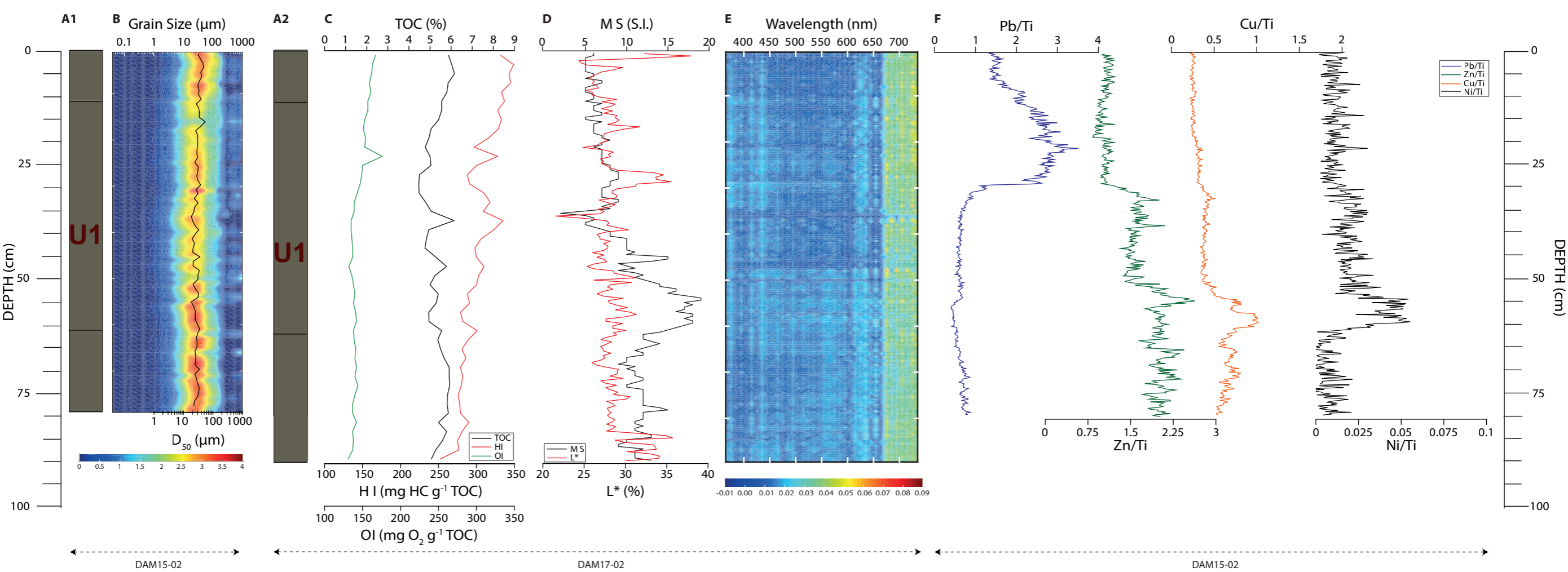
Figure S11. Correlation matrix with XRF core scanning data (Al, Si, Fe, Ti, Mn, Zn, Cu, Ni, and Pb), TOC, and grain size (D_{50} , clay ($< 2 \mu\text{m}$), silt ($2\text{-}63 \mu\text{m}$), and coarse fraction ($> 63 \mu\text{m}$)) from the Eure Unit of the MAR15-01 core (Pearson correlation, p-value < 0.001 for all the $R < -0.6$ and $R > 0.6$).

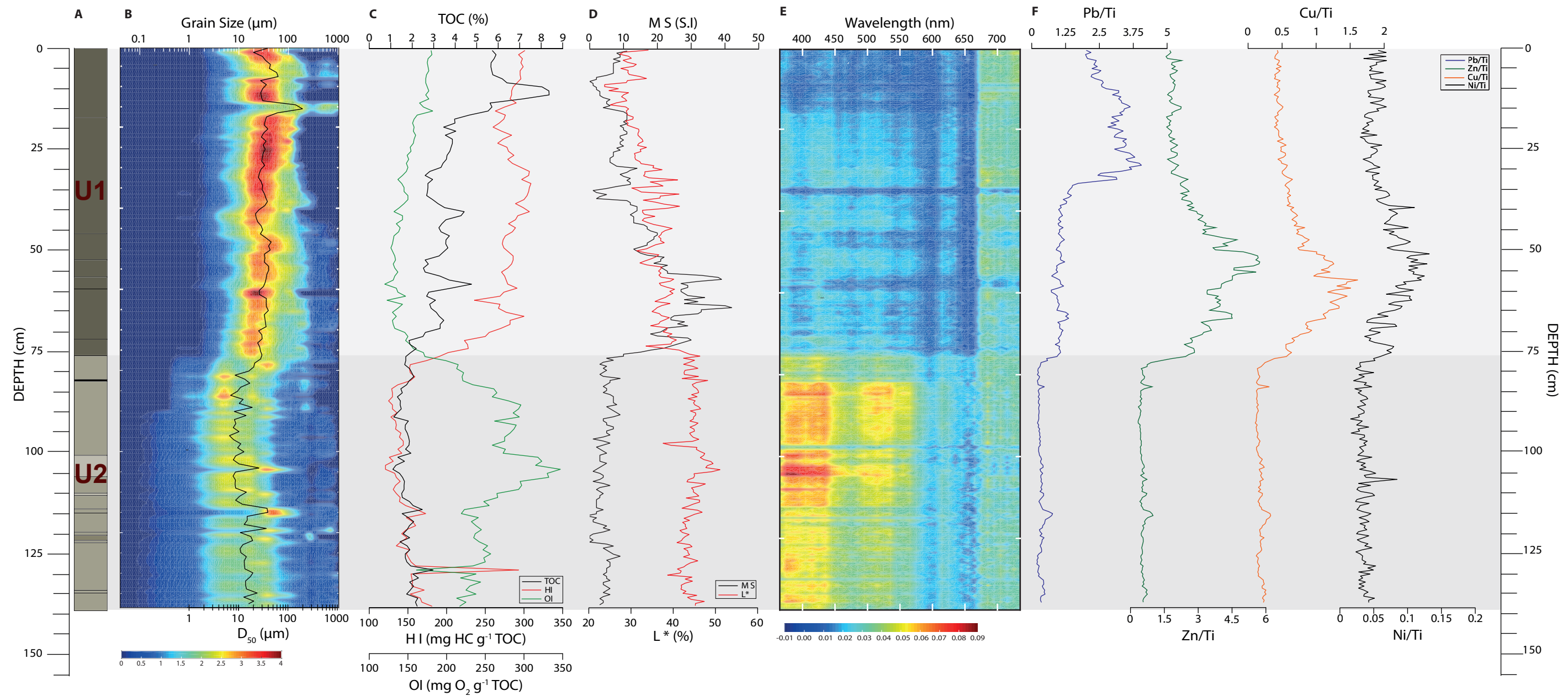
Tableau 1. Characteristics of sediment cores collected in Les Damps Pond and Martot Pond (WGS 84).

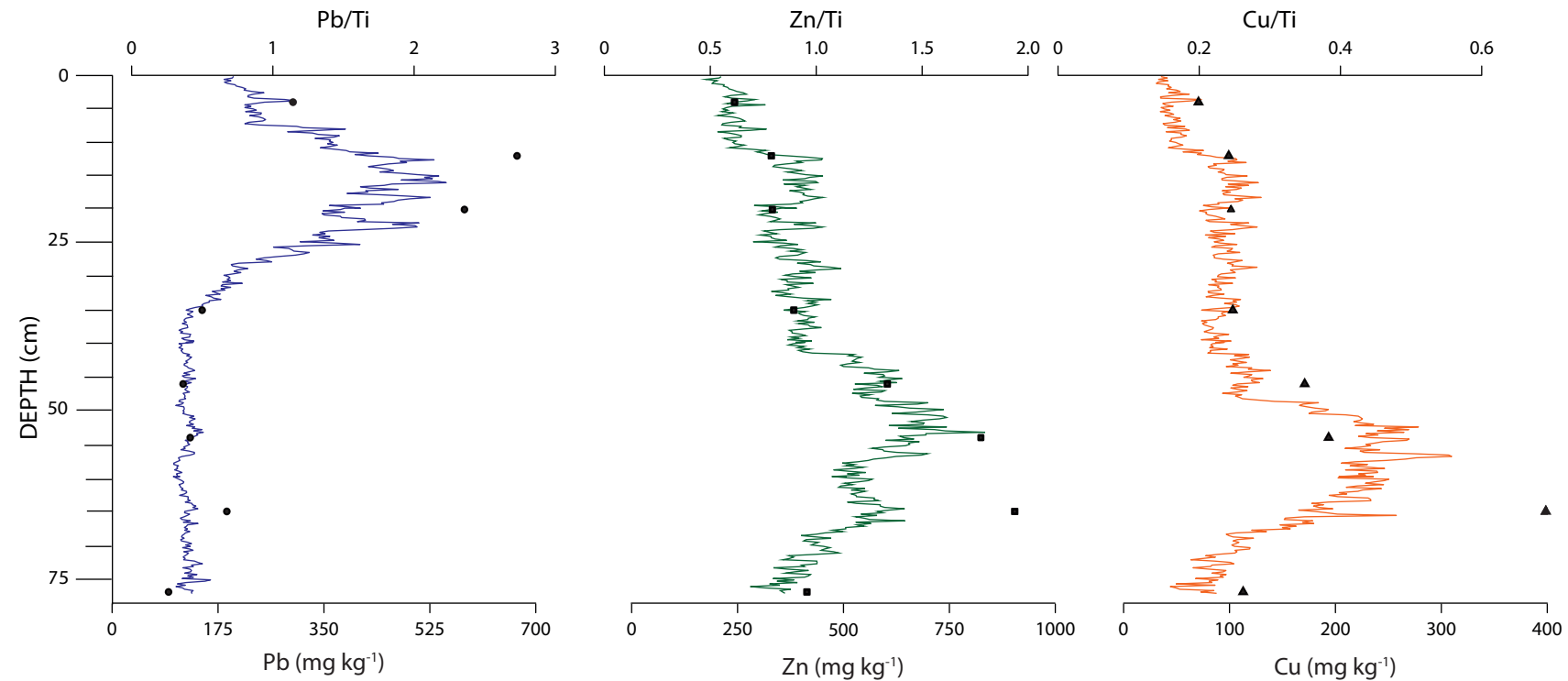


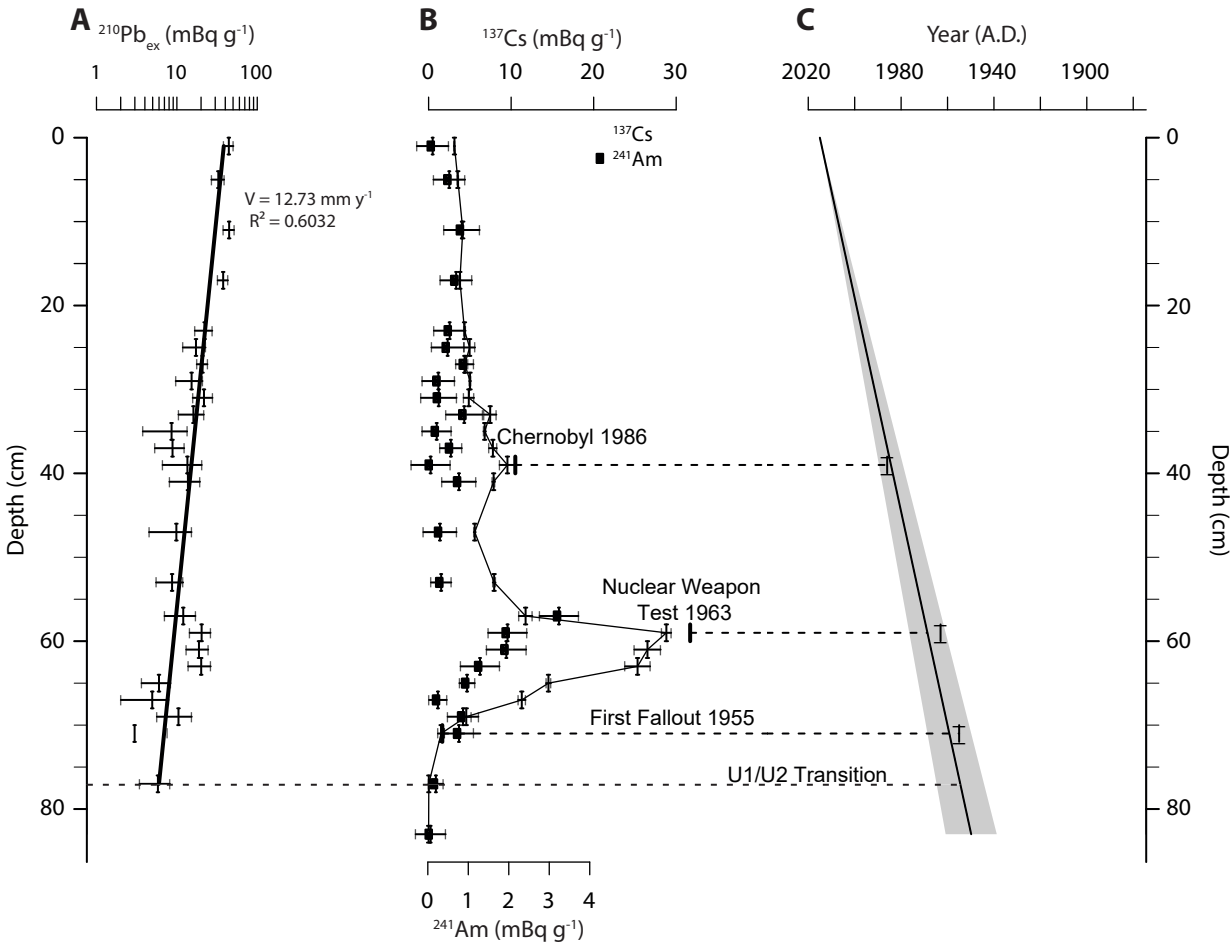


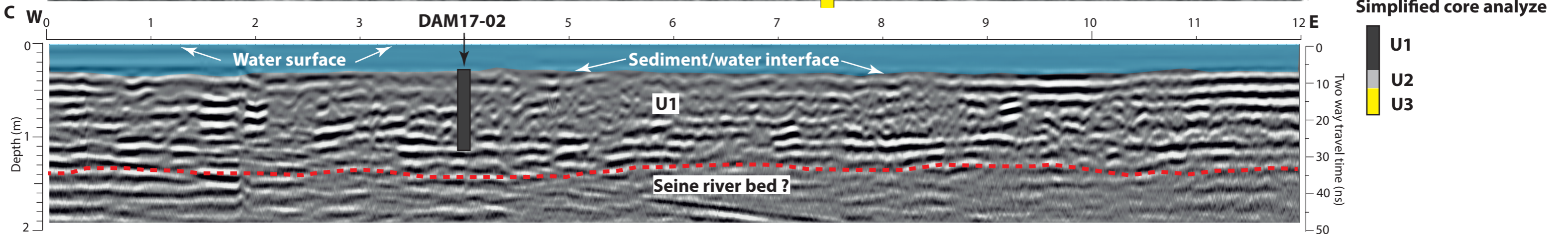
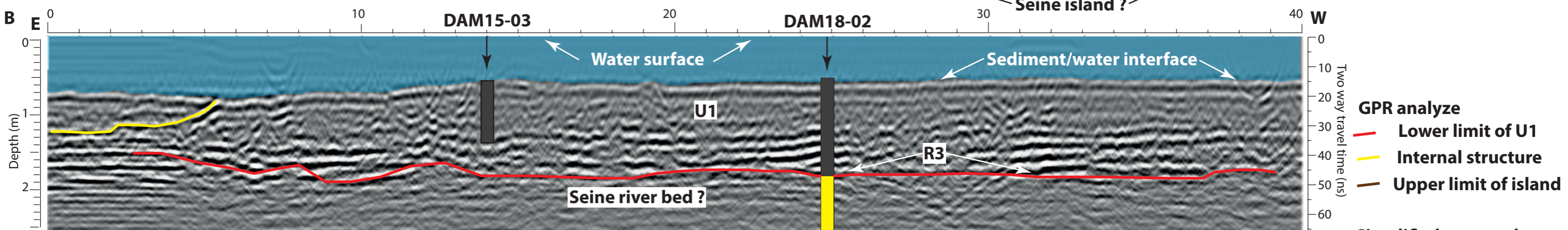
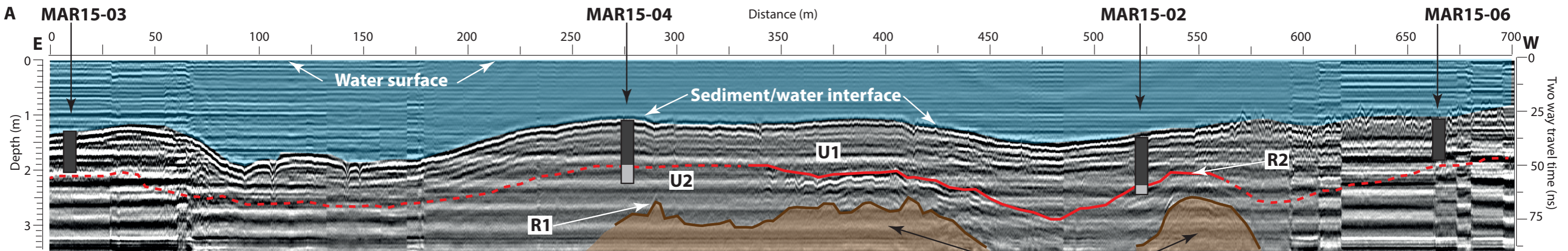


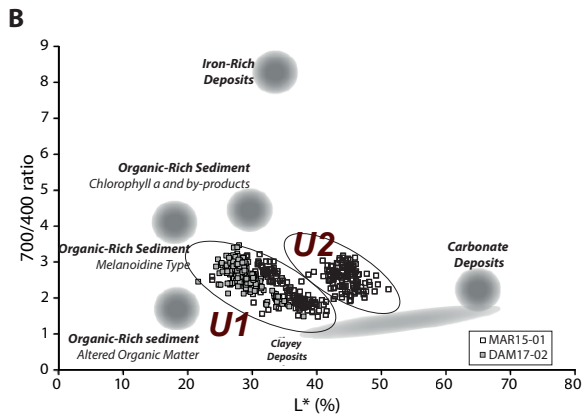
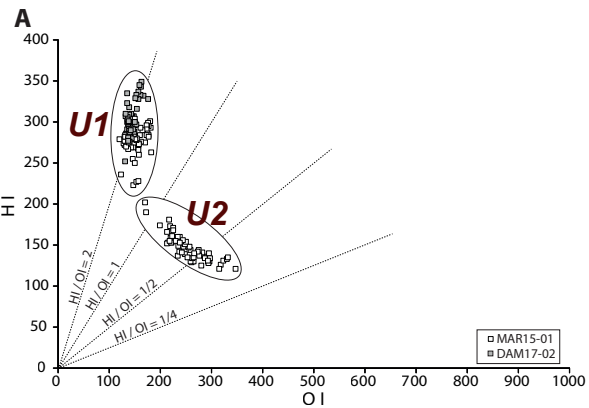


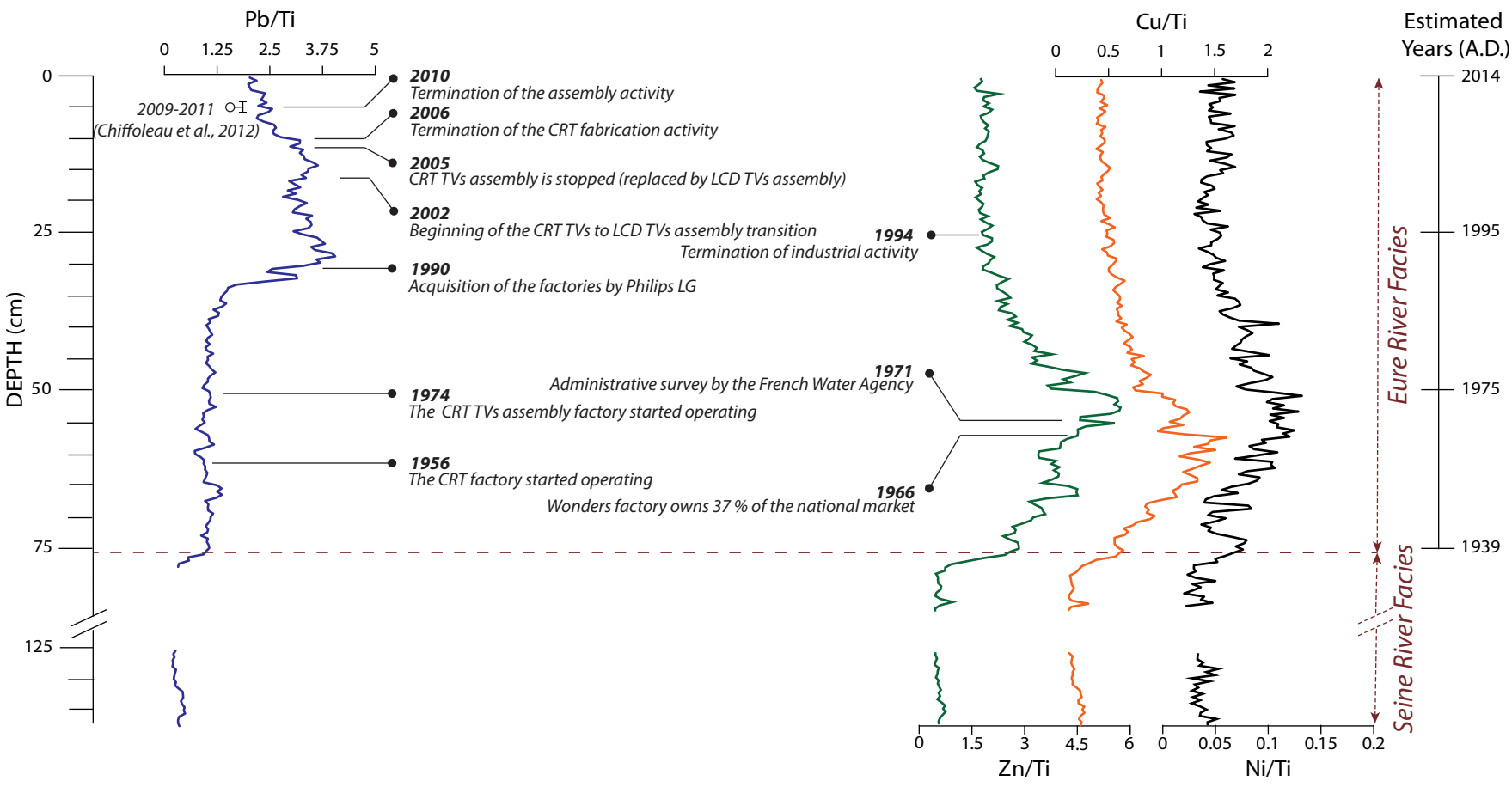












Pond	Core ID	IGSN	Longitude (X)	Latitude (Y)	Core Length (cm)
LES DAMPS (DAM)	DAM15-02	IEM2C0016	1°10'9.05" E	49°18'16.13" N	80
	DAM15-03	IEM2C0017	1°10'11.58" E	49°18'15.83" N	67
	DAM17-02	IEM2C000E	1°10'13.26" E	49°18'15.66" N	90
	DAM18-02	IEM2C001C	1°10'11.14" E	49°18'16.09" N	208
MARTOT (MAR)	MAR15-01	IEM2C0001	1°03'1.68" E	49°17'49.68" N	138
	MAR15-02	IEM2C0002	1°03'12.49" E	49°17'50.63" N	93
	MAR15-03	IEM2C0003	1°03'30.45" E	49°18'1.69" N	68
	MAR15-04	IEM2C0004	1°03'23.34" E	49°17'54.44" N	104
	MAR15-05	IEM2C0005	1°03'2.84" E	49°17'49.69" N	161
	MAR15-06	IEM2C0006	1°03'5.49" E	49°17'49.88" N	96
	MAR16-02	IEM2C0008	1°03'2.60" E	49°17'49.30" N	129